# BOSE-EINSTEIN CONDENSATION OF MAGNONS IN FERROMAGNETS AND ANTIFERROMAGNETS

by

PETRO ARTEMCHUK

A dissertation submitted in partial fulfillment of the
requirements for the degree of

DOCTOR OF PHILOSOPHY IN APPLIED AND COMPUTATIONAL PHYSICS

2025

Oakland University
Rochester, Michigan

Doctoral Advisory Committee:

Andrei Slavin, Ph.D., Chair
Vasyl Tyberkevych, Ph.D., Co-Chair
Gopalan Srinivasan, Ph.D.
Alexey Tonyushkin, Ph.D.

*To my mother and grandmother.*

# ACKNOWLEDGMENTS

The author wishes to express his appreciation for extensive mentorship provided by Andrei Slavin, my adviser, and Vasyl Tyberkevych, who provided additional research guidance. Thanks are also due to committe members Gopalan Srinivasan, Ph.D and Alexei Tonyushkin, Ph.D for their contributions to this dissertation.

Petro Artemchuk

ABSTRACT

BOSE-EINSTEIN CONDENSATION OF MAGNONS IN FERROMAGNETS AND ANTIFERROMAGNETS

by

Petro Artemchuk

Adviser: Andrei Slavin, Ph.D.

Bose-Einstein condensation is a collective phenomenon which is the process of transition of many bosons - particles having integer spin - to the same coherent quantum state. One of the examples of bosons are magnons - the quanta of spin waves propagating in magnetic media. Formation of Bose-Einstein condensate (BEC) of magnons has been observed experimentally in ferromagnetic (FM) materials and analyzed in theory. The peculiarity is that BEC of magnons can be formed at room temperature.

The BEC of magnons exhibits dynamic properties related to transport of magnon density, which appears to be anisotropic. In addition, the BEC of magnons also possesses nonlinear properties related to interaction of magnons in BEC and responsible for its stability. However, the theory available does not take into account all the important factors.

Antiferromagnetic materials (AFM) also allow for existence of magnons, which implies the possibility of BEC formation in AFM materials as well. Although such a possibility has been discussed multiple times, none of the methods proposed has been realized on practice yet.

The dissertation first informs about relevant topics, covering principles of magnonics, formation of BEC and its properties. It then describes a model aimed to describe both transport and nonlinear properties of magnons in BEC while accounting for all the peculiarities of magnons. After this, it explores in theory the interaction of magnon

gas in the process of BEC formation with an isolated low-frequency mode. Finally, it delves into formation of BEC in AFM samples using a method of rapid cooling. It analyzes conditions required for BEC formation and discusses possible practical realization.

The research presented in the dissertation helps to understand complicated phenomena related to formation and existence of BEC. It also opens new possibilities and directions of research both theoretical and experimental ones.

TABLE OF CONTENTS

LIST OF TABLES

LIST OF FIGURES

# LIST OF ABBREVIATIONS

| | |
|---|---|
| AFM | Antiferromagnetic |
| AFMR | Antiferromagnetic Resonance |
| BEC | Bose-Einstein Condensate |
| FM | Ferromagnetic |
| SEV | Spin Excitation Vector |
| VHF | Vector Hamiltonian Formalism |

# CHAPTER ONE

# INTRODUCTION

## 1.1 Motivation

Bose-Einstein condensation is a collective phenomenon which manifests itself through transition of many bosons - particles with integer value of spin - into the same quantum state. The resulting coherent accumulation of bosons is called Bose-Einstein condensate (BEC). A widely know example of BEC formation is superconductivity of electrons in metals at cryogenic temperatures due to merging of electrons into Cooper pairs having integer value of spin. Another example is superfluidity of Helium at criogenic temperatures. Magnons are quasi particles having spin equal one. In contrary to the above mentioned cases, they can form BEC at room temperature, which makes magnon BEC much more convenient to investigate. Magnon BEC has properties related to transport of magnon density and to nonlinear interaction between magnons, which is responsible for stability of magnon BEC. These properties were observed experimentally and were explained in theory. Some explanations however do not take into account peculiarities of thickness profiles of magnon modes.

## 1.2 Organization of the dissertation

Chapter 2 contains background information relevant to topics discussed in the dissertation. It starts with introduction to the field of magnonics and the phenomenon of BEC. It tells about nature of magnons and their properties in FM and AFM materials. Then, it discusses the process of formation of BEC and methods which either were used in experiments or the ones proposed in theory.

Chapters 3-5 cover the original results obtained for this dissertation. These results were presented in 18 conference presentations [1], [2], [3], [4], [5], [6], [7], [8], [9], [10], [11], [12], [13], [14], [15], [16], [17] and one invited talk [18].

Chapter 3 presents a model aimed to explain transport and nonlinear properties of magnons in the state of BEC in thick magnetic films. It discusses how anisotropy of magnon dispersion leads to anisotropy of properties of magnons. The chapter ends with derivation of coefficients of nonlinear interaction for the case of thick magnetic films and analysis of nonlinear frequency shift.

Chapter 4 delves into interaction of magnon gas in the process of BEC formation with an isolated nonlinear mode. It discusses peculiarities of such interaction and introduces a new model accounting for discrepancies between known theory and the case of coherent mode involved.

Chapter 5 considers the use of method of rapid cooling for creation of magnon BEC in AFM materials. The chapter provides the model suitable for description of temporal evolution of magnon gas, describes the obtained results and discusses the practical realization.

Chapter 6 provides overview of the theoretical models described in the dissertation and summarizes the results they lead to. The chapter ends with discussion of potential directions for future research.

# CHAPTER TWO

# BACKGROUND

## 2.1 Magnonics

### 2.1.1 Ferromagnets

Magnetic materials are divided into several classes according to their magnetic properties, which are closely related to their atomic stricture. Ferromagnetic (FM) materials (ferromagnets) have spontaneous magnetization even in the absence of applied magnetic field. Depending on the size of the sample the ground state can be a single-domain or a multi-domain one. Single-domain sample has its magnetization pointing in mostly the same direction over the whole sample. In this case the exchange interaction between magnetic moments is dominant. The single-domain state is usually observed for samples of small size. Multi-domain ground state appears when the size is large and dipolar interaction become more important. Magnetic sample is trying to minimize its energy which leads to splitting of a single domain into multiple smaller domains separated by domain walls. If an external magnetic field is applied, FM will magnetize in the direction of applied magnetic field with consideration of possible anisotropy fields. If deviation of magnetic moment from its equilibrium direction occurs, the magnetic moment will start to precess around the direction of the applied magnetic field. This perturbation can propagate along the chain of magnetic moments and create a magnetic excitation - a spin wave. Spin wave can be described by taking into account the magnitude of the magnetization precession and phase of precession of magnetic moments participating in it.

When the problem to solve does not require to know in details microscopic dynamic of magnetic moments, spin wave can be described as a quasi-particle - magnon.

When magnons are used, one can focus on macroscopic parameters of a system considered and describe spin waves in terms of populations of specific magnon modes. The disadvantage of the magnon approach is that the information about phase of a spin wave is lost. The phases of spin waves are important as they help to understand the connection between spin waves, whether they will amplify or suppress each other in the case of interaction (will the interference between them be constructive or destructive). This is also important when the nature of a magnetic excitation is discussed.

Magnons are quanta of spin waves similar to electrons being quanta of electric charge. To describe one spin wave of specific amplitude one would need to use certain number of magnons. They would also need to be careful and remember that the magnons the spin wave consists of are coherent, which makes them similar to spin waves having he same phase of oscillation. In some case one needs to consider incoherent magnons. Incoherent magnons are similar to spin waves having different phases. An example of incoherent magons are thermal magnons existing in a magnetic sample due to finite temperature of environment. The populations of such magnons satisfy the Bose-Esintein distribution. Although the populations of thermal magnons can be significant, they are usually completely incoherent, their complex amplitudes have random phases so thermal magnons of the same frequency do not create spin waves. The distinction between coherent and incoherent mangons is quite important as they would require different equations for proper description of interaction between them.

### 2.1.2 Antiferromagnets

Antiferromagnetic (AFM) materials, in contrary to FM, do not have total magnetic moment in the equilibrium state. In terms of atomic structure, they effectively have two sublattices magnetized in opposite direction and thus compensating each other. AFM are known to barely interact with the applied magnetic field. Since AFM have two effective sublattices, their magnon spectrum consists of two branches, which may be degenerate or not depending on the type of AFM. An important distinction between FM and AFM magnons is the magnitude of magnon frequency. AFM have stronger exchange interaction which leads to AFM magnon frequencies of the order of 1 THz rather than 1 GHz (3 order of magnitude difference). Another important difference is that AFM magnon spectrum is isotropic due to negligible dipolar interaction.

## 2.2 Bose-Einstein condensation of magnons

Bose-Einstein condensation of magnons is a collective phenomenon which corresponds to transition of a huge amount of boson particles into the same quantum state. In this state all the bosons are described by the same wave function. An important distinction between formation of Bose-Einstein Condensate (BEC) and simply amplification of an excitation or accumulation of a large number of particles is that BEC is formed spontaneously (there is no process of adding particles directly into BEC) under specific conditions.

Magnons are bosons having spin equal 1. This implies the possibility of magnons undergoing the process of Bose-Einstein condensation. In most cases Bose-Einstein condensation requires criogenic temperatures for the process to happen. The examples of this are the electrons combining into Cooper pairs, thus, creating boson particles, which leads to superconductivity in metals, and superfluidity of Helium III. Magnons on the other hand can have transition into BEC at room temperature due to their small effective mass, which makes them convenient to investigate.

### 2.2.1 Bose-Einstein condensation of magnons in ferromagnets

Bose-Esintein condensation of magnons was first experimentally observed when a parametrcially driven gas of magnons has been studied [19]. In this case magnons are added to the system using method of parametric pumping. The pumped magnons undergo process of thermalization during which magnons interact with each other through 4-magnon processes and with lattice. Thermalization of high-frequency magnons leads to creation of significant amount of low-frequency magnons. The sample made of Yittrium Iron Garnet (YIG) is characterized by a long magnon lifetime, which is much less then the thermalization time. This leads to accumulation of magnons at the bottom of the spectrum, which increases the chemical potential of the magnon gas. Due to the form of Bose-Einstein distribution, the condition for BEC formation is an increase of chemical potential of magnons gas to the level corresponding to minimum energy of magnons in the spectrum.

The method of parametric pumping is not the only way to achieve Bose-Einstein condensation of magnons. BEC of magnons was later achieved in experiment involving rapid cooling of a thin magnetic film made of YIG [20]. In this experiment, the source of high energy magnons are the non equilibrium thermal magnons created by simply heating up the part of the area of the magnetic film. In the process of rapid cooling of the film the sample itself (the lattice) cools down during time of the order of 1 ns. The magnon gas, however, cools down with the rate that depends on properties of the magnon gas itself, specifically, intensity of magnon interaction. The very term "rapid cooling" means that sample cools down faster than the magnons gas. Due to difference in cooling rate between lattice and magnon gas, for a short period of time the sample is populated with non-equilibrium high-frequency thermal magnons. These non-equilibrium magnon undergo process of thermalization similar to magnons added using method of parametric pumping, which then leads to accumulation of low-energy magnons and increase of chemical potential of the magnon gas. The latter makes the condition for BEC formation satisfied, which was observed experimentally.

In addition to parametric pumping and rapid cooling, possible ways to create and control BEC of magnons include spin Hall effect [21], [22], which is, essentially, an injection of spin current leading to spin torque pumping.

### 2.2.2 Transport properties of BEC

The state of BEC is characterized by significantly increased magnon density which can be observed experimentally and have its evolution tracked in time [20]. When magnon BEC is created in a part of the sample, it can be imagined as a spot with increased magnon density. Due to phase gradient, the area of increased magnon density will move and grow in size. During this "expansion" magnon BEC demonstrates anisotropic transport properties, meaning, propagation of magnons density along the applied magnetic field is more intense then in the direction perpendicular to it. Such anisotropy is mainly due to anisotropy of the magnon spectrum in FM materials.

### 2.2.3 Nonlinear properties of BEC

In addition to transport of magnon density (dynamic properties), BEC of magnons also possesses nonlinear properties. The source of these nonilnear properties is the 4-magnon interaction between magnons inside BEC.

It should be noted that in the case of applied in-plane magnetic field, the magnon spectrum is anisotropic and the minimum of magnon energy is not at the zero wavevector, which is different from the case of ferromagnetic resonance (FMR). Instead, there are two minima located at nonzero wavevector in the direction corresponding to the direction of the applied in-plane magnetic field.

Since the spectrum of magnons has two minima created by interplay between exchange and dipolar interaction, BEC of magnons is actually two BECs located at two minima of the spectrum. Although we talk about magnons being located in different minima of the spectrum, they only separated in the momentum space as their wavevctors have opposite directions. In the real space magnons from both spectral minima coexist together in the same part of the sample. It was, however, demonstrated that one can separate the two components of magnon BEC and observe their motion int time [23].

The coexistence of two BEC components leads to two types of nonlinear interaction: self- and cross- interaction. Self- interaction corresponds to interaction between magnons of the same kind while cross-interaction describes interaction between magnons belonging to different minima of the spectrum.

Nonlinear properties of magnon BEC are very important for existence of BEC as they, essentially, define its stability.

2.2.4 Bose-Einstein condensation of magnons in antiferromagnets

Although AFM materials barely interact with the applied magnetic field, they still have magnons. The possibility of Bose-Einstein condensation of magnons in AFM has been discussed several times mostly involving theoretical derivations. There are also reports of experiments when observed data could be explained by Bose-Einstein condensation of magnons. Those experiment, however, were done at millikelvin temperatures.

One of the reasons why BEC of magnons in AFM is important to investigate is that minima of AFM spectrum branches correspond to sub-TH and THz frequencies. Considering the fact that BEC is a coherent state of particular magnon energy (and thus, magnon frequency), Bose-Esintein condensation in AFM is potentially a key to a new technology of generation of sub-THz pulses.

# CHAPTER THREE

# DESCRIPTION OF DYNAMIC AND NONLINEAR PROPERTIES OF BOSE-EINSTEIN CONDENSATION OF MAGNONS IN FERROMAGNETS

In this chapter dynamic and nonlinear properties of magnons in the state of Bose-Einstein condensate (BEC) are discussed. A model to describe such properties of magnons in BEC at the condensation point at the bottom of the spectrum is derived. A thin-film geometry sample is considered as it is commonly used in experiments. In addition, the magnetic film is considered to be "thick" in a sense of its thickness being much greater than the exchange length of the magnetic material, which is a typical situation when the method of parametric pumping [24] is used.

The results discussed in this chapter were previously presented in conference presentations [1], [3], [4], [5].

## 3.1 Description of magnetization dynamics using vector Hamiltonian formalism

To describe magnetization dynamics as well as properties of the system in this chapter, a method of Vector Hamiltonian Formalism (VHF)[25] is utilized. This approach is suitable for description for weakly nonlinear dynamics in magnetic systems.

The peculiarity of the magnetization description is in projecting the spherical space of the magnetization vector $\mathbf{m}$ into a plane. When spatial distribution of magnetization over a magnetic sample is considered, at each point $\mathbf{r}$ we project magnetization $\mathbf{m}(t,\mathbf{r})$ from the unit sphere into the plane and obtain the Spin Excitation Vector (SEV) $\mathbf{s}(t,\mathbf{r})$ orthogonal to the ground state magnetization $\mathbf{m}_0$. In this case, the magnetization $\mathbf{m}(t,\mathbf{r})$ can be calculated as:

$$\mathbf{m} = \left(1 - \frac{s^2}{2}\right)\mathbf{m}_0 + \sqrt{1 - \frac{s^2}{4}}\,\mathbf{s}, \tag{3.1}$$

where $s = |\mathbf{s}|$ is the SEV $\mathbf{s}$.

The SEV itself can be calculated from the ground state $\mathbf{m}_0$ and the magnetization $\mathbf{m}$ using the transformation:

$$\mathbf{s} = \hat{\mathbf{P}}_0 \cdot \mathbf{m} + \frac{1 - \mathbf{m}_0 \cdot \mathbf{m}}{4} \hat{\mathbf{P}}_0 \cdot \mathbf{m}_0, \tag{3.2}$$

where $\hat{\mathbf{P}}_0$ is the projection operator into the SEV plane:

$$\hat{\mathbf{P}}_0 \equiv \hat{\mathbf{I}} - \mathbf{m}_0 \otimes \mathbf{m}_0. \tag{3.3}$$

The particular equations used will be introduced as derivations are described.

## 3.2 Magnon dispersion in BEC region

General VHF equations for eigen-modes:

$$-i\omega_\nu \hat{\mathbf{L}}_0 \cdot \mathbf{s}_\nu = \hat{\mathbf{H}}_0 \cdot \mathbf{s}_\nu, \tag{3.4}$$

Here

$$\hat{\mathbf{L}}_0 \cdot \mathbf{x} = -L_s \mathbf{m}_0 \times \mathbf{x}, \hat{\mathbf{H}}_0 = \hat{\mathbf{P}}_0 \cdot \left(\hat{\mathbf{H}} + M_s B_0 \hat{\mathbf{I}}\right) \cdot \hat{\mathbf{P}}_0, \tag{3.5}$$

$$\hat{\mathbf{P}}_0 = \hat{\mathbf{I}} - \mathbf{m}_0 \otimes \mathbf{m}_0, \tag{3.6}$$

$L_S = M_S/\gamma$, where $M_S$ is the saturation magnetization, $\gamma$ is the gyromagnetic ratio, $B_0$ is the scalar internal magnetic field applied along the $x$-axis (see Fig. 3.1), $\hat{\mathbf{H}}$ is the operator describing self-interactions in the system and $\hat{\mathbf{H}}_0$ is the linear Hamiltonian of the system.

For dipole-exchange spin waves in films, the energy operator in $\mathbf{k}$-representation ($\mathbf{k}$ is the in-plane wavevector) is

$$\hat{\mathbf{H}}_\mathbf{k} = -\mu_0 M_s^2 \lambda_{ex}^2 \hat{\nabla}_\mathbf{k}^2 + \mu_0 M_s^2 \hat{\mathbf{G}}_\mathbf{k}, \tag{3.7}$$

where $\mu_0$ is the vacuum permeability, $\lambda_{\mathrm{ex}}$ is the exchange length, $\hat{\nabla}_{\mathbf{k}}^2 = -k^2 + d^2/dz^2$, $z$ is the coordinate normal to the film, and $\hat{\mathbf{G}}_{\mathbf{k}}$ is the dipolar operator:

$$\begin{aligned}\hat{\mathbf{G}}_{\mathbf{k}}(z,z') = \frac{k}{2}e^{-k|z-z'|}\hat{\mathbf{k}}\hat{\mathbf{k}} + i\frac{k}{2}\mathrm{sign}(z-z')e^{-k|z-z'|}(\hat{\mathbf{k}}\hat{\mathbf{z}} + \hat{\mathbf{z}}\hat{\mathbf{k}}) \\ + \left(\delta(z-z') - \frac{k}{2}e^{-k|z-z'|}\right)\hat{\mathbf{z}}\hat{\mathbf{z}}.\end{aligned} \tag{3.8}$$

Here $\hat{\mathbf{k}}$ is the unit vector in the direction of $\mathbf{k}$.

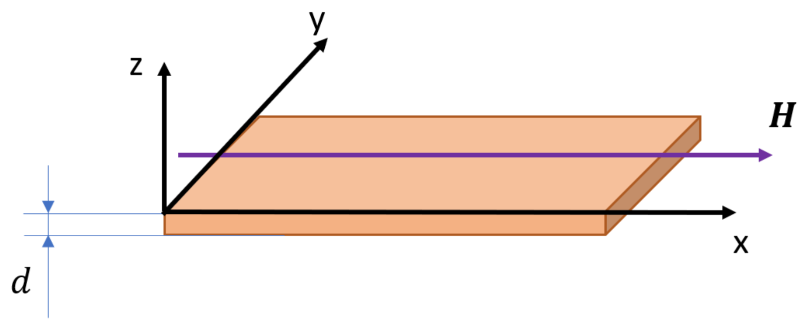


Figure 3.1: Geometry of sample considered for description of dynamic and nonlinear properties of BEC of magnons. The sample is a thin film of thickness $d$ made of FM material. The sample is in-plane magnetized by magnetic field $\mathbf{H} = \mathbf{B}/\mu_0$ applied in the $x$-direction, where $\mu_0$ is the vacuum permeability.

To describe properties of magnons in the state of BEC, a thin-film geometry sample of thickness $d$ (see Fig. 3.1) is considered. The sample is magnetized by an external magnetic field and the ground state of magnetization is described by a vector field $\mathbf{m}_0(\mathbf{r})$ and scalar internal magnetic field $B_0(\mathbf{r})$, The sample is considered to be uniformly magnetized so both $\mathbf{m}_0$ and $B_0$ are constant (independent of coordinates): $\mathbf{m}_0(\mathbf{r}) = \mathbf{m}_0$, $B_0(\mathbf{r}) = B_0$. The eigen-mode profiles $\mathbf{s}_\nu(z)$ ($\nu = (\mathbf{k}, n)$, where $n$ is the eigen-mode profile number, can be expanded using some orthogonal system of "thickness functions" $f_j(z)$:

$$\mathbf{s}_\nu(z) = \sum_j c_j f_j(z), \tag{3.9}$$

$$\frac{1}{d}\int_0^d f_j(z) f_{j'}(z) dz = \Delta_{j,j'} \tag{3.10}$$

(we assume that $f_j(z)$ are real-valued). Then, the VHF equations become an infinite system of equations for coefficients $\mathbf{c}_{\nu,j}$:

$$-i\omega_\nu \hat{\mathbf{L}}_0 \cdot \mathbf{c}_{\nu,j} = \sum_{j'} \hat{\mathbf{H}}_{0,(j,j')} \cdot \mathbf{c}_{\nu,j'}. \tag{3.11}$$

Here

$$\hat{\mathbf{H}}_{0,(j,j')} = \hat{\mathbf{P}}_0 \cdot \left(\hat{\mathbf{H}}_{j,j'} + M_s B_0 \hat{\mathbf{I}}\right) \cdot \hat{\mathbf{P}}_0, \tag{3.12}$$

$$\hat{\mathbf{H}}_{j,j'} = \frac{1}{d}\int_0^d f_j(z) \hat{\mathbf{H}}_{\mathbf{k}} f_{j'}(z') dz. \tag{3.13}$$

If the choice of $f_j(z)$ is close to real eigen-mode profiles, the diagonal approximation can be applied:

$$-i\omega_\nu \hat{\mathbf{L}}_0 \cdot \mathbf{c}_{\nu,j} = \hat{\mathbf{H}}_{0,(j,j)} \cdot \mathbf{c}_{\nu,j}. \tag{3.14}$$

Depending on the distribution of the magnetization precession amplitude over a magnetic film thickness, the thickness functions $f_j(z)$ may need to satisfy requirement of pinned spins (magnetization at the surface does not precess) or unpinned spins (magnetization at the surface has non-zero angle of precession). It has been shown [26], that in the BEC region, the appropriate choice of $f_j(z)$ are the functions satisfying the requirement of pinned spin:

$$f_j(z) = \sqrt{2} \sin\left(\kappa_j z\right), \tag{3.15}$$

where $\kappa_j = \pi j/d$. Then,

$$\hat{\mathbf{H}}_{j,j} = \mu_0 M_s^2 \lambda_{\text{ex}}^2 q_j^2 \hat{\mathbf{I}} + \mu_0 M_s^2 \left( P_j \hat{\mathbf{k}}\hat{\mathbf{k}} + (1-P_j)\hat{\mathbf{z}}\hat{\mathbf{z}} \right), \tag{3.16}$$

where $P_j$ the result of integration of the part of the dipolar operator:

$$\begin{aligned} P_j = \frac{1}{d}\int_0^d f_j(z)\left[\int_0^d \frac{k}{2} e^{-k|z-z'|} f_j(z')dz'\right] dz = \\ = \frac{k^2}{q_j^2} + \frac{2\kappa_j^2 k}{q_j^4 d}\left[1-(-1)^j e^{-kd}\right]. \end{aligned} \tag{3.17}$$

Here $q_j$ is the total (3D) wavenumber: $q_j^2 = k^2 + \kappa_j^2$. In the BEC region, $kd \gg 1$ and $P_j$ can be approximated as

$$P_j \approx 1 - \frac{\kappa_j^2}{k^2}. \tag{3.18}$$

Below the index $j$ is dropped for simplicity (dependence on $j$ is described by the dependence on $\kappa$). For the BEC geometry, magnetization is in-plane, and we choose $\mathbf{m}_0 = \hat{\mathbf{x}}$. Complex amplitude $\mathbf{c}$ can then be decomposed into the $y$ and $z$ components:

$$\mathbf{c} = \alpha\hat{\mathbf{y}} + i\beta\hat{\mathbf{z}}. \tag{3.19}$$

Then,

$$\hat{\mathbf{H}}_0 \cdot \mathbf{c} = L_{\text{s}}(\omega_{\text{B}} + \omega_{\text{M}}\lambda_{\text{ex}}^2 q^2)(\alpha\hat{\mathbf{y}} + i\beta\hat{\mathbf{z}}) + L_{\text{s}}\omega_{\text{M}}(P_k \sin^2\phi_k \alpha\hat{\mathbf{y}} + i(1-P_k)\beta\hat{\mathbf{z}}), \tag{3.20}$$

where $\phi_k$ is the in-plane propagation angle relative to $\mathbf{m}_0$ ($\hat{\mathbf{k}} = \cos\phi_k\hat{\mathbf{x}} + \sin\phi_k\hat{\mathbf{y}}$). By introducing notation

$$\omega_\alpha = (\omega_{\text{B}} + \omega_{\text{M}}\lambda_{\text{ex}}^2 q^2 + \omega_{\text{M}}(1-P_k))\beta, \tag{3.21}$$

$$\omega_\beta = (\omega_{\text{B}} + \omega_{\text{M}}\lambda_{\text{ex}}^2 q^2 + \omega_{\text{M}} P_k \sin^2\phi_k)\alpha, \tag{3.22}$$

equation (3.20) can be rewritten as

$$\hat{\mathbf{H}}_0 \cdot \mathbf{c} = L_{\mathrm{s}} \left( \omega_\beta \hat{\mathbf{y}} + i\omega_\alpha \hat{\mathbf{z}} \right) \tag{3.23}$$

Considering Eq. (3.23) and diagonal approximation for $\hat{\mathbf{H}}_0$, the eigen-frequency of $\hat{\mathbf{H}}_0$ can be found from equation $\omega^2 = \omega_\alpha \omega_\beta / (\alpha\beta)$:

$$\omega^2 = (\omega_{\mathrm{B}} + \omega_{\mathrm{M}}\lambda_{\mathrm{ex}}^2 q^2 + \omega_{\mathrm{M}}(1 - P_k))(\omega_{\mathrm{B}} + \omega_{\mathrm{M}}\lambda_{\mathrm{ex}}^2 q^2 + \omega_{\mathrm{M}} P_k \sin^2\phi_k). \tag{3.24}$$

The ellipticity $\varepsilon$ of propagating spin waves can be found from ratio of components of the complex amplitude $\mathbf{c}$:

$$\varepsilon = \frac{\beta}{\alpha} = \left( \frac{\omega_{\mathrm{B}} + \omega_{\mathrm{M}}\lambda_{\mathrm{ex}}^2 q^2 + \omega_{\mathrm{M}} P_k \sin^2\phi_k}{\omega_{\mathrm{B}} + \omega_{\mathrm{M}}\lambda_{\mathrm{ex}}^2 q^2 + \omega_{\mathrm{M}}(1 - P_k)} \right)^{1/2} \tag{3.25}$$

## 3.3 Thick film approximation

Although the sample considered has a thin-film geometry, its thickness can be considered to be much larger than the exchange length ($d \gg \lambda_{\mathrm{ex}}$). Especially this is true for the films used in experiments utilizing parametric pumping. For such "thick" films the bottom of the spectrum - BEC point - is at the wavenumber $k_{\mathrm{min}}$, which satisfies inequalities:

$$1/\lambda_{ex} \gg k_{\mathrm{min}} \gg 1/d \tag{3.26}$$

Also, BEC corresponds to magnon propagating along the applied magnetic field $B_0$, hence, $\sin\phi_k = 0$. In this case, the dispersion can be approximated as

$$\omega \approx \omega_{\mathrm{B}} + \omega_{\mathrm{M}}\lambda_{\mathrm{ex}}^2 k^2 + \omega_{\mathrm{M}} \frac{\xi^4}{d^2} k^{-2}, \tag{3.27}$$

where $\xi = (\pi/\sqrt{2})^{1/2} \approx 1.49$.

The BEC point is located in the minimum of the spectrum and for dispersion above the minimum is at the wavenumber

$$k_{\min} = \frac{\xi}{\sqrt{\lambda_{\mathrm{ex}} d}}. \tag{3.28}$$

The BEC frequency at the BEC point is

$$\omega_{\min} = \omega_{\mathrm{B}} + 2\xi^2 \omega_{\mathrm{M}} \frac{\lambda_{\mathrm{ex}}}{d}. \tag{3.29}$$

and the ellipticity $\varepsilon$ is close to 1 at the BEC point.

## 3.4 Parabolic approximation of dipersion at the BEC point

Near the BEC point, the dispersion can be approximated as parabola,

$$\omega \approx \omega_{\min} + \frac{D_{\parallel}}{2}(k - k_{\min})^2, \tag{3.30}$$

where $\omega_{\min}$ and $k_{\min}$ are the angular frequency and wavenumber of magnons at the bottom of the magnons spectrum, where the BEC of magnons is formed.

The coefficient for dispersion in the x-direction (along the direction of applied magnetic field) $D_{\parallel}$ can be calculated as

$$D_{\parallel} = \frac{\partial^2 \omega}{\partial {k_x}^2} = 8\omega_M \lambda_{\mathrm{ex}}^2. \tag{3.31}$$

We can also calculate dispersion in the $y$-direction, which lies in the plane of the magnetic film perpendicular to the applied magnetic field ($\mathbf{k} = k_{\min}\hat{\mathbf{x}} + k_y\hat{\mathbf{y}}$):

$$\omega \approx \omega_{\min} + \frac{D_{\perp}}{2} k_y^2, \tag{3.32}$$

$$D_{\perp} = \omega_M k_{\min}^{-2} = \xi^{-2} \omega_M \lambda_{ex} d, \tag{3.33}$$

where $k_y$ is a small deviation of the magnon wavevector from the BEC point in the $y$-direction.

It should be noted that the ratio of between coefficients of dispersion parallel and along the applied magnetic field is

$$\frac{D_\perp}{D_\parallel} = \frac{d}{8\xi^2\lambda_{ex}} \gg 1, \tag{3.34}$$

which implies anisotropy of properties of magnons at the BEC point.

Finally, we can consider the frequency as a function of $\kappa$ - effective wavenumber in the normal-to-film direction:

$$\omega \approx \omega_{\text{min}} + \frac{1}{2}\omega_{\text{M}}\frac{\kappa^2 - \kappa_1^2}{k_{\text{min}}^2}, \tag{3.35}$$

from which one can find the dispersion coefficient related to $\kappa$:

$$D_\kappa = \omega_{\text{M}}/k_{\text{min}}^2 = D_\perp. \tag{3.36}$$

As one can see, in the approximation used dispersion coefficient related to out-of-plane direction is equal to the one in the in-plane direction perpendicular to the applied magnetic field.

It should be noted that the effective wavenumber $\kappa$ is actually quantized and is related to thickness modes in film. The thickness modes are similar to the quantized energy levels of a particle in an infinite potential well: change of $\kappa$ and transfer from one branch of the magnon spectrum to another is an analogue of a particle moving from one energy level to another in an infinite potential well. In this sense, the magnon in the state of BEC can be interpreted as BEC boson in infinite potential well $0 < z < d$ (a thick film acts as a potential well), where bosons have dispersion:

$$\omega_{\mathbf{k}} = \left(\omega_{\text{B}} + \xi^2\omega_{\text{M}}\frac{\lambda_{\text{ex}}}{d}\right) + \frac{1}{2}(\mathbf{K} - \mathbf{K}_{min}) \cdot \hat{\mathbf{D}} \cdot (\mathbf{K} - \mathbf{K}_{\text{min}}), \tag{3.37}$$

where $\mathbf{K}$ is the 3D boson wavevector, $\mathbf{K}_{\text{min}} = \pm k_{\text{min}}\hat{\mathbf{x}}$ for minima located at $k_{\text{x}} > 0$ and $k_{\text{x}} < 0$ and $\hat{\mathbf{D}}$ is the dispersion matrix describing anisotropic effective mass of magnons: $\hat{\mathbf{D}} = \text{diag}(D_{\parallel}, D_{\perp}, D_{\perp})$.

## 3.5 Nonlinear interaction between magnons in BEC

### 3.5.1 Description of nonlinear interaction between magnons in BEC

As was discussed in Chapter 2, there are two types of nonlinear interactions between magnon present in BEC: the self-interaction between magnon located in the same spectral minimum and the cross-interaction between magnon located in different minima. The aim of this chapter is to find simple expressions for nonlinear coefficients of self- and cross-interaction between magnons in BEC and discuss their meaning. A number of approximations related to the problem considered has been used:

- assumption of totally pinned spins [26];
- all magnons are described as identical eigenmodes having the same thickness profile;
- magnons propagate parallel to the applied magnetic field in the plane of the film in the direction of the $x$-axis;
- the sample is assumed to be uniformly magnetized with magnetization $\mathbf{m}$ directed along the $x$-axis in the ground state;
- eigenmodes in BEC have ellipticity $\varepsilon = 1$.

The energy of four-magnon nonlinear interaction can be written using symmetrized nonlinear coefficient $W_{\alpha\beta\gamma\delta}$ [25]:

$$H_4 = \frac{1}{24} \sum_{\alpha\beta\gamma\delta} W_{\alpha\beta\gamma\delta} c_\alpha c_\beta c_\gamma c_\delta, \tag{3.38}$$

where $c_\nu$ is the dimensionless complex amplitude describing the profile of an eigenmode having eigenfrequency $f_\nu$ and angular eigenfrequency $\omega_\nu = 2\pi f_\nu$:

$$c_\nu = e^{i\omega_\nu t} \tag{3.39}$$

.

The general expression for the coefficient $W_{\alpha\beta\gamma\delta}$ is

$$W_{\alpha\beta\gamma\delta} = \tilde{W}_{\alpha\beta,\gamma\delta} + \tilde{W}_{\alpha\gamma,\beta\delta} + \tilde{W}_{\alpha\delta,\beta\gamma}, \tag{3.40}$$

where $\tilde{W}_{\alpha\beta,\gamma\delta}$ is the non-symmetrized nonlinear coefficient described in general by expression:

$$\begin{aligned}\tilde{W}_{\alpha\beta,\gamma\delta} = \int \Big( &(\mathbf{s}_\alpha \cdot \mathbf{s}_\beta)\mathbf{m}_0 \cdot \hat{\mathbf{H}} \cdot ((\mathbf{s}_\alpha \cdot \mathbf{s}_\beta)\mathbf{m}_0) - \frac{1}{4}(\mathbf{s}_\alpha \cdot \mathbf{s}_\beta)\mathbf{s}_\gamma \cdot \hat{\mathbf{H}} \cdot \mathbf{s}_\delta \\ &- \frac{1}{4}(\mathbf{s}_\alpha \cdot \mathbf{s}_\beta)\mathbf{s}_\delta \cdot \hat{\mathbf{H}} \cdot \mathbf{s}_\gamma - \frac{1}{4}(\mathbf{s}_\gamma \cdot \mathbf{s}_\delta)\mathbf{s}_\alpha \cdot \hat{\mathbf{H}} \cdot \mathbf{s}_\beta - \frac{1}{4}(\mathbf{s}_\gamma \cdot \mathbf{s}_\delta)\mathbf{s}_\beta \cdot \hat{\mathbf{H}} \cdot \mathbf{s}_\alpha \Big) d\mathbf{r},\end{aligned} \tag{3.41}$$

where $\hat{\mathbf{H}}$ is the integral operator

$$\hat{\mathbf{H}} \cdot \mathbf{s}_\nu \equiv \int_V \hat{\mathbf{H}}(\mathbf{r}, \mathbf{r}') \cdot \mathbf{s}_\nu(\mathbf{r}') d\mathbf{r}'. \tag{3.42}$$

In Eqs. (3.41) and (3.42), $\mathbf{s}_\nu$ is the SEV representing the eigenmode having a specific spatial and thickness profiles:

$$\mathbf{s}_\nu = a_\nu \mathbf{S}_\nu f_\nu(z) e^{(i\mathbf{k}_\nu \cdot \rho)}, \tag{3.43}$$

where $a_\nu$ is the normalization constant, $\mathbf{S}_\nu = (0, 1, i\varepsilon_\nu)$ is the SEV which describes magnetization direction and depends on the ellipticity of the eigenmode $\varepsilon_\nu$, and $f_\nu(z)$ is the thickness profile of the eigenmode.

Considering the SEV in a form (3.43), peculiarities of integral operator $\hat{\mathbf{H}}$ and the fact that all the eigen-mode interacting have the same thickness profile and normalization constant, the simplified expressions for separate terms of Eq. (3.41) can be obtained:

$$\begin{aligned}&\int(\mathbf{s}_\alpha\cdot\mathbf{s}_\beta)\mathbf{m}_0\cdot\hat{\mathbf{H}}\cdot((\mathbf{s}_\gamma\cdot\mathbf{s}_\delta)\mathbf{m}_0)d\mathbf{r}=\\&=a_\nu^4(\mathbf{S}_\alpha\cdot\mathbf{S}_\beta)(\mathbf{S}_\gamma\cdot\mathbf{S}_\delta)A_{x,y}\frac{1}{d}\int_0^d f(z)^2\mathbf{m}_0\cdot(\hat{\mathbf{H}}_{k\gamma+k_\delta}\cdot\mathbf{m}_0 f(z')^2)dz\end{aligned}\tag{3.44}$$

$$\int(\mathbf{s}_\alpha\cdot\mathbf{s}_\beta)\mathbf{s}_\gamma\cdot\hat{\mathbf{H}}\cdot\mathbf{s}_\delta d\mathbf{r}=a_\nu^4(\mathbf{S}_\alpha\cdot\mathbf{S}_\beta)\mathscr{A}_{x,y}\frac{1}{d}\int_0^d f(z)^3\mathbf{S}_\gamma\cdot(\hat{\mathbf{H}}_{k_\delta}\cdot\mathbf{S}_\delta f(z'))dz,\tag{3.45}$$

where $\mathscr{A}_{\mathrm{x,y}}$ is the area in $xy$ plane over which the integral is taken, and $\hat{\mathbf{H}}_k$ is the integral operator $\hat{\mathbf{H}}$ written for a specific value of a wavevector $k$.

Considering the expression for operator $\hat{\mathbf{H}}_k$ the common factor can be taken outside using substitution

$$\hat{\mathbf{H}}_k=\mu_0 M_s\hat{\mathbf{H}}'_k.\tag{3.46}$$

The form of Eq. (3.41) can be simplified by introducing new integral operators $A_{\gamma,\delta}$ and $B_{\gamma,\delta}$:

$$A_{\gamma,\delta}=\int_0^d f(z)^2\mathbf{m}_0\cdot\left(\hat{\mathbf{H}}'_{k\gamma+k_\delta}\cdot\mathbf{m}_0 f(z')^2\right)dz;\tag{3.47}$$

$$B_{\gamma,\delta}=\int_0^d f(z)^3\mathbf{S}_\gamma\cdot\left(\hat{\mathbf{H}}'_{k_\delta}\cdot\mathbf{S}_\delta f(z')\right)dz,\tag{3.48}$$

using which one can write the expression for nonlinear factor $\tilde{W}_{\alpha\beta,\gamma\delta}$ in a form:

$$\begin{aligned}&\tilde{W}_{\alpha\beta,\gamma\delta}=a_\nu^4\mathscr{A}_{x,y}\frac{\mu_0 M_s^2}{d^2}\Bigg((\mathbf{S}_\alpha\cdot\mathbf{S}_\beta)\cdot(\mathbf{S}_\gamma\cdot\mathbf{S}_\delta)A_{\gamma,\delta}\\&-\frac{1}{2}\left[(\mathbf{S}_\alpha\cdot\mathbf{S}_\beta)B_{\gamma,\delta}+(\mathbf{S}_\alpha\cdot\mathbf{S}_\beta)B_{\delta,\gamma}+(\mathbf{S}_\gamma\cdot\mathbf{S}_\delta)B_{\alpha,\beta}+(\mathbf{S}_\gamma\cdot\mathbf{S}_\delta)B_{\beta,\alpha}\right]\Bigg).\end{aligned}\tag{3.49}$$

Next, the normalization constant $a_\nu$ must be found. According to VHF, $a_\nu$ is defined by condition of orthogonality between eigenmodes:

$$\frac{M_s}{\gamma}\int\mathbf{s}_\nu^*\cdot\hat{\mathbf{J}}\cdot\mathbf{s}_\nu d\mathbf{r}=-i\hbar_\nu\delta_{\nu,\nu'},\tag{3.50}$$

where $\hat{\mathbf{J}}$ is the operator that has matrix form

$$\hat{\mathbf{J}} = \begin{pmatrix} 0 & m_{0,z} & -m_{0,y} \\ -m_{0,z} & 0 & m_{0,x} \\ m_{0,y} & -m_{0,x} & 0 \end{pmatrix} \tag{3.51}$$

and $\hbar_\nu$ is the real-valued norm of the $\nu$-th mode [25]:

$$\hbar_\nu \equiv -i \int_V \mathbf{s}_\alpha^* \cdot \hat{\mathbf{L}}_0 \cdot \mathbf{s}_\alpha d\mathbf{r}. \tag{3.52}$$

The value of $\hbar_n u$ can be chosen as $\hbar\nu = \hbar$, where $\hbar$ is the reduced Planck constant. This corresponds to the quasi-classical "magnon" normalization when the mode profile $\mathbf{s}_\nu$ is a classical analog of a magnon wavefunction and the number of magnons in the mode is equal to the mode amplitude squared.

Considering the assumption regard the norm $\hbar_\nu$ and the fact that interacting modes $c_\nu$ and $c_{\nu'}$ are essentially the same (except propagation in opposite directions), the calculation of the normalization constant $a_\nu$ yields

$$a_\nu = i\sqrt{\frac{\gamma\hbar d}{2M_s \mathbf{m}_{0,x}^2 \varepsilon_\nu \mathscr{A}_{x,y} F'_{\nu,\nu}}}, \tag{3.53}$$

which transforms the common factor in Eq. (3.49):

$$a_\nu^4 \mathscr{A}_{x,y} \frac{\mu_0 M_s^2}{d^2} = \frac{\mu_0 \gamma^2 \hbar^2}{4\mathbf{m}_{0,x}^2 \varepsilon_\nu^2 \mathscr{A}_{x,y} F'_{\nu,\nu}}, \tag{3.54}$$

where $F'_{\nu,\nu} = \int_0^d f_\nu^2(z)dz$. For simplicity, we introduce notation

$$\mathscr{W}_\nu = \frac{\mu_0 \gamma^2 \hbar^2}{4\mathbf{m}_{0,x}^2 \varepsilon_\nu^2 \mathscr{A}_{x,y} (F'_{\nu,\nu})^2} \tag{3.55}$$

By taking into account that all the modes interacting have the same thickness profiles and ellipticity, the index $\nu$ can be omitted in the normalization constant and the common factor:

$$a_\nu \equiv a = i\sqrt{\frac{\gamma\hbar d}{2M_s\mathbf{m}_{0,x}^2\varepsilon\mathscr{A}_{x,y}F'}}; \tag{3.56}$$

$$\mathscr{W}_\nu \equiv \mathscr{W} = \frac{\mu_0\gamma^2\hbar^2}{4\mathbf{m}_{0,x}^2\varepsilon^2\mathscr{A}_{x,y}(F')^2} \tag{3.57}$$

After taking all the common factors outside the parenthesis, the expressions inside can be simplified.First, the properties of the operator $\hat{\mathbf{H}}_k$ must be taken into account. Some of the terms in parenthesis turns out to be the same, because, considering the assumptions,

$$\mathbf{S}_\gamma \cdot \hat{\mathbf{H}}'_{k_\delta} \cdot \mathbf{S}_\delta = \mathbf{S}_\delta \cdot \hat{\mathbf{H}}'_{k\gamma} \cdot \mathbf{S}_\gamma. \tag{3.58}$$

Since complex amplitudes $\mathbf{S}_\nu$ do not depend on coordinate $z$ (this dependence is taken care of by spin wave profile functions $f_\nu(z)$), the integral operators $A_{\gamma,\delta}$ and $B_{\gamma,\delta}$ introduced in (3.45) and (3.46) are symmetric:

$$A_{\gamma,\delta} = A_{\delta,\gamma} = A_{\gamma\delta}; \tag{3.59}$$

$$B_{\gamma,\delta} = B_{\delta,\gamma} = B_{\gamma,\delta}. \tag{3.60}$$

This allows to write three equations describing terms in Eq. (3.49) required for calculation of coefficient of nonlinear interaction between magnons. After simplifications described above Eq. (3.49) transforms into

$$\begin{aligned}\hat{\mathbf{W}}_{\alpha\beta,\gamma\delta} = \mathscr{W}\Big( &(\mathbf{S}_\alpha \cdot \mathbf{S}_\beta)(\mathbf{S}_\gamma \cdot \mathbf{S}_\delta)A_{\gamma\delta} \\ &- \frac{1}{4}[(\mathbf{S}_\alpha \cdot \mathbf{S}_\beta)2B_{\gamma\delta}) + (\mathbf{S}_\gamma \cdot \mathbf{S}_\delta)2B_{\alpha\beta})]\Big)\end{aligned} \tag{3.61}$$

Equation (3.61) still preserves different indexes for complex amplitudes of interacting magnon modes, while similarity in other parameters has been taken into account.

To define coefficient of nonlinear self- and cross- interaction, index $\nu$ is assigned to magnons propagating in positive direction ($k_x > 0$) and index $\tilde{\nu}$ is assigned to magnons propagating in opposite direction ($k_x < 0$). Thus, using Eq. (3.40), the coefficients of nonlinear self-interaction $W_{\text{self}}$ and nonlinear cross-interaction $W_{\text{cross}}$ can be defined:

$$W_{\text{self}} = W_{\nu\nu\nu^*\nu^*} = \tilde{W}_{\nu\nu,\nu^*\nu^*} + \tilde{W}_{\nu\nu^*,\nu\nu^*} + \tilde{W}_{\nu\nu^*,\nu\nu^*}; \tag{3.62}$$

$$W_{\text{cross}} = W_{\nu\tilde{\nu}\nu^*\tilde{\nu}^*} = \tilde{W}_{\nu\tilde{\nu},\nu^*\tilde{\nu}^*} + \tilde{W}_{\nu\nu^*,\tilde{\nu}\tilde{\nu}^*} + \tilde{W}_{\nu\tilde{\nu}^*,\tilde{\nu}\nu^*}. \tag{3.63}$$

Considering properties of complex amplitudes $\mathbf{S}_\nu$ and the fact that in the BEC region magnonic modes have ellipticity $\varepsilon = 1$, final expressions for nonlinear coefficients $W_{\text{self}}$ and $W_{\text{cross}}$ have the form:

$$W_{\text{self}} = -2\mathscr{W} B_{\nu\nu^*}; \tag{3.64}$$

$$W_{\text{cross}} = \mathscr{W}\left(\tilde{A}_0 + \tilde{A}_{2k} - 2B_{\nu\nu^*}\right), \tag{3.65}$$

where $\tilde{A}_0 = A^*_{\nu^*\tilde{\nu}} = A_{\tilde{\nu}\tilde{\nu}^*}$, $\tilde{A}_{2k} = A_{\tilde{\nu}\nu^*}$, while $B_{\nu\nu^*}$ and $\mathscr{W}$ are defined by () and () correspondingly.

3.5.2 Nonlinearity of magnon interaction in the case of arbitrary demagnetization tensor

The previous subsection was dedicated to derivation of nonlinear coefficients of self- and cross-interaction between magnons. Although equations do not look complicated, they are still written for a general case, the particular parameters of the operator $\hat{\mathbf{H}}_k$ have not been specified. This subsection is dedicated to a particular case of sample having certain demagnetization tensor $\hat{\mathbf{N}}$. Lets remind ourselves the form of the normalized integral operator $\hat{\mathbf{H}}'$ in the $k$-space:

$$\hat{\mathbf{H}}'_k(z,z') = -\lambda_{ex}^2 \nabla_k^2 \hat{\mathbf{I}} + \hat{\mathbf{G}}_k, \tag{3.66}$$

where $\nabla_k$ is the nabla operator:

$$\nabla_k^2 = -k^2 + \frac{\partial^2}{\partial z^2} \tag{3.67}$$

In the case of the same geometry (thin magnetic film), but specific in-plane dimensions, length $a$ and width $b$ (see Fig. 3.2), dipolar energy tensor $\hat{\mathbf{G}}_k$ will be diagonal. The operator $\hat{\mathbf{G}}_k$ corresponds to averaged Green function. By multiplying it over magnetization and averaging it over the whole sample, one can obtain demagnetizing field. Considering that the magnetization of the sample is assumed to be uniform and $\hat{\mathbf{H}}$ is normalized by $\mu_0 M_s$, the energy due to demagnetization field be written as $M_s^2$ multiplied by integral denoting averaging of the Green function (here it is averaged over the the film thickness as initially the film was considered infinite). This approach can be generalized by substituting traditional diagonal demagnetization tensor instead of the average Green function. The fact that in the and result will be demagnetization field energy is supported by appearance of $M_s^2$ in the normalization constant in front of the expression for nonlinear coefficient (it is included into $\tilde{\mathscr{W}}$).

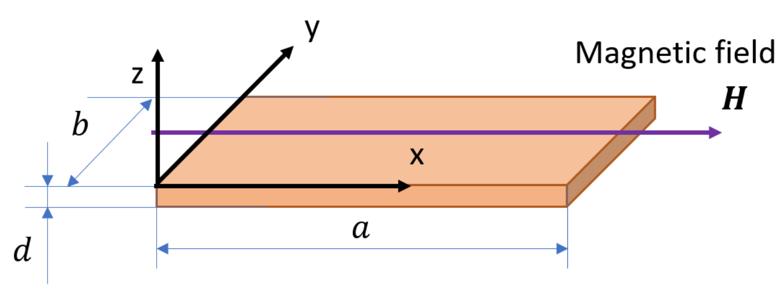


Figure 3.2: Geometry of a thin film sample with finite in-plane dimensions. The film of thickness $d$ has length $a$ and width $b$.

Integration of (3.66) yields

$$\int \hat{\mathbf{H}}_k' dz dz' = -\int \lambda_{ex}^2 \nabla_k^2 \hat{\mathbf{I}} + \hat{\mathbf{N}}, \tag{3.68}$$

where integration over the exchange part denotes any integration performed with consideration of of the thickness profiles of eigenmodes. Instead of performing integration the whole, one may use known results instead. Operator $\hat{\mathbf{N}}$ represents demagnetization tensor, which in the diagonal case, can be written as

$$\hat{\mathbf{N}} = \begin{pmatrix} N_x & 0 & 0 \\ 0 & N_y & 0 \\ 0 & 0 & N_y \end{pmatrix}, \tag{3.69}$$

where demagnetization factors $N_x$ and $N_y$ depend on dimensions of the sample:

$$N_{\mathrm{x}} \sim \frac{d}{a}; \qquad N_{\mathrm{y}} \sim \frac{d}{b}. \tag{3.70}$$

It should be taken into account that the sample considered has a geometry of a thin films. Here the assumption of a thin film simply means that the area of the film is much larger than the thickness of the film, which helps to make assumption about particular values of demagnetization factors. The film is still considered thick in terms of physics of magnetism: the thickness of the film $d$ is much larger than the exchange length $\lambda_{ex}$. Thus we assume that components of the demagnetization tensor are

$$N_x = \zeta_x, \qquad N_y = \zeta_y, \qquad N_z = 1 - \zeta_x - \zeta_y, \tag{3.71}$$

where $\zeta_x$ and $\zeta_y$ are small parameters denoting in-plane demagnetization of a magnetic film.

Another important detail to consider is that propagating spin waves (magnons) feel the influence of demagnetizing field completely different from the case of uniform precession of magnetization. In the case of spin waves demagnetization tensor can be calculated as

$$\hat{\mathbf{N}}_{sw} = \frac{\mathbf{k}\otimes\mathbf{k}}{|\mathbf{k}|^2} = \frac{1}{|\mathbf{k}|^2}\begin{pmatrix} k_x^2 & k_xk_y & k_xk_z \\ k_yk_x & k_y^2 & k_yk_z \\ k_zk_x & k_zk_y & k_z^2 \end{pmatrix}. \tag{3.72}$$

Since magnons in BEC only have nonzero $x$-component of the wavevector, the "spin-wave" demagnetization tensor $\hat{\mathbf{N}}_{sw}$ has the form

$$\hat{\mathbf{N}}_{sw} = \begin{pmatrix} 1 & 0 & 0 \\ 0 & 0 & 0 \\ 0 & 0 & 0 \end{pmatrix}. \tag{3.73}$$

By taking into account peculiarities of demagnetization tensor, nonlinear coefficients for the lowest eigenmode ($\kappa = \pi/d$) can be calculated:

$$W_{\text{self}} = -4\tilde{W}\left(3\lambda_{ex}^2 k_{\text{min}}^2 - \beta^2\pi^2 - 2\zeta_x\right); \tag{3.74}$$

$$W_{\text{cross}} = 4\tilde{W}\left(\beta^2\pi^2 + \zeta_x + 3\lambda_{\text{ex}}^2 k_{\text{min}}^2 + 1\right), \tag{3.75}$$

where $k_{BEC}$ is the wavenumber for magnons in BEC and $\beta = \lambda_{ex}/d$ is a small parameter.

Substitution of $k_{\text{min}}$ into Eqs. (3.76) and (3.75) yields

$$W_{\text{self}} = -2\mathscr{W}\left(3\xi^2\beta - \beta^2\pi^2 - 2\zeta_x\right); \tag{3.76}$$

$$W_{\text{cross}} = 4\mathscr{W}\left(\beta^2\pi^2 + \zeta_x + 3\xi^2\beta + 1\right), \tag{3.77}$$

where $\xi \approx 1.49$. It should be noted that the demagnetization factor $\zeta_y$ is absent in the expressions obtained, which implies that under used assumptions demagnetization in-plane perpendicular to the direction of propagation of magnons (which is also the direction of the applied magnetic field) does not affect the nonlinear interaction between magnons.

Considering that $\beta$ and $\zeta_x \equiv N_x$ are small parameters ($\beta \ll 1$ ,$\zeta_x \ll 1$) we can further simply expressions by keeping only first-order terms for the self-interaction factor and only dominant term for cross-interaction factor:

$$W_{\text{self}} = 4\mathscr{W}\left(2N_x - 3\xi^2\beta\right); \tag{3.78}$$

$$W_{\text{cross}} = 4\mathscr{W}, \tag{3.79}$$

where the common factor $\mathscr{W}$ is simplified due to the assumptions used:

$$\mathscr{W} = \frac{\gamma^2\hbar^2\mu_0}{V} \tag{3.80}$$

where $V$ is the volume of the considered thin-film sample.

3.5.3 Nonlinear frequency shift due to interaction between magnons

The nonlinear frequency shift due to either self- or cross-interaction between magnons is proportional to the product of the correspondent nonlinear coefficient $W$ and population of magnons $n$ in BEC. However, it would be convenient to characterize the nonlinear shift relative to the maximum possible magnon population $n_{\text{max}}$:

$$\Delta\omega_{\text{self/cross}} = \Omega_{\text{self/cross}}\frac{n}{n_{\text{max}}}, \tag{3.81}$$

where $\Delta\omega_{\text{self/cross}}$ is the nonlinear shift due to self-/cross- interaction between magnons.

The maximum possible magnon population can be calculated from the material parameters:

$$n_{\text{max}} = \frac{2L_{\text{s}}}{\hbar}, \tag{3.82}$$

where $L_{\text{s}}$ is the spin that corresponds to saturation magnetization $M_s$:

$$L_{\text{s}} = \frac{M_{\text{s}}}{\gamma}, \tag{3.83}$$

where $\gamma$ is the gyromagnetic ratio. Together (3.80) and (3.82) give us

$$n_{\text{max}} = \frac{2M_{\text{s}}}{\gamma\hbar}. \tag{3.84}$$

Considering (3.81) and (3.84) we get

$$\Omega_{\text{self/cross}} = \frac{W_{\text{self/cross}}}{\hbar} V n_{\text{max}}, \tag{3.85}$$

which, with consideration of (3.76), (3.77) and (3.80) gives us

$$\Omega_{\text{self}} = 8\gamma\mu_0 M_{\text{s}} \left[2N_x - 3\xi^2\beta\right], \tag{3.86}$$

$$\Omega_{\text{cross}} = 8\gamma\mu_0 M_{\text{s}}\pi. \tag{3.87}$$

The expression for the total nonlinear frequency shift with consideration of symmetry of nonlinear factors can be derived with consideration of the Hamiltonian $\mathscr{H}$ of BEC of magnons:

$$\begin{aligned} \mathscr{H} = \hbar\omega_\nu(c_\nu c_\nu^* + c_{\nu'} c_{\nu'}^*) + \frac{1}{4} W_{\nu\nu\nu^*\nu^*} c_\nu c_\nu c_\nu^* c_\nu^* \\ + \frac{1}{4} W_{\nu'\nu'\nu'^*\nu'^*} c_{\nu'} c_{\nu'} c_{\nu'}^* c_{\nu'}^* + \frac{1}{2} W_{\nu\nu\nu'^*\nu'^*} c_\nu c_{\nu'} c_\nu^* c_{\nu'}^* \end{aligned} \tag{3.88}$$

The equation of motion in the Hamiltonian form is

$$i\hbar \frac{dc_\nu}{dt} = \frac{\partial \mathscr{H}}{\partial c_\nu^*} \tag{3.89}$$

By applying Eq. (3.89) to Eq. (3.88) the equation of motion becomes

$$i\hbar \frac{dc_\nu}{dt} = \hbar\omega'_{\text{min}} c_\nu, \tag{3.90}$$

where $\omega'_{\text{min}}$ is the BEC magnon frequency with consideration of nonlinear shift:

$$\omega'_{\text{min}} = \omega_\nu + \frac{1}{4\hbar}\left(W_{\text{self}} n_{\text{self}} + 2W_{\text{cross}} n_{\text{cross}}\right), \tag{3.91}$$

where $n_{\text{self}} = n_1, n_{\text{cross}} = n_2$ if equation is written for magnons having $k_x > 0$, and $n_{\text{self}} = n_2, n_{\text{cross}} = n_1$ if equation is written for magnons having $k_x < 0$. Specifically, $n_1$

and $n_2$ are the partial magnon densities of magnon BEC in the minima of the FM magnon spectrum ($n_1$ is the density of magnons in BEC at $k_x = k_{\text{min}}$ and $n_2$ is the density of magnons in BEC at $k_x = -k_{\text{min}}$).

Considering Eqs. (3.85) and the fact that $\omega_v \equiv \omega_{\text{min}}$, we can rewrite the frequency $\omega$ in terms of relative magnon density $n/n_{\text{max}}$:

$$\omega'_{\text{min}} = \omega_{\text{min}} + \frac{1}{4}\left(\Omega_{\text{self}} + 2\Omega_{\text{cross}}\right)\frac{n}{n_{\text{max}}}, \tag{3.92}$$

where populations of magnons in both minima are considered to be the same: $n = n_1 = n_2$.

The expression can be further by taking into account the expression for $n_{\text{max}}$ and the common factor of $1/4$:

$$\omega'_{\text{min}} = \omega_{\text{min}} + \left(\tilde{\Omega}_{\text{self}} + 2\tilde{\Omega}_{\text{cross}}\right)n, \tag{3.93}$$

where

$$\tilde{\Omega}_{\text{self}} = \gamma^2\hbar\mu_0\left[2N_x - 3\xi^2\beta\right], \tag{3.94}$$

$$\tilde{\Omega}_{\text{cross}} = \gamma^2\hbar\mu_0. \tag{3.95}$$

The Eq. (3.93) can be generalized for the case of different magnon densities of magnon BECs located in different minima of the FM spectrum of magnons:

$$\omega'_{\text{min}} = \omega_{\text{min}} + \left(\tilde{\Omega}_{\text{self}}n_{\text{self}} + 2\tilde{\Omega}_{\text{cross}}n_{\text{cross}}\right), \tag{3.96}$$

where, again, where $n_{\text{self}} = n_1, n_{\text{cross}} = n_2$ if equation is written for magnons having $k_x > 0$, and $n_{\text{self}} = n_2, n_{\text{cross}} = n_1$ if equation is written for magnons having $k_x < 0$.

## 3.6 Conclusion

In conclusion, the model presented allows one to consider magnons in the BEC as boson quasy-particles in a potential well, whose effective mass is characterized by a tensor and depends on the dispersion law at the spectral minima. Simple expressions for the BEC point (spectral minimum) and the correspondent longitudinal wavevector magnitude has been found and can be used for quick estimation of magnetic film thickness required to observe BEC of magnons at a particular frequency/longitudinal wavevector. To account for nonlinear effect, coefficient of nonlinear self- and cross interaction between magnons have been found as well as resulting nonlinear frequency shift. The expressions for nonlinear coefficients are in a good agreement with results found by other authors and show the influence of the dimensions of the film on the stability of magnon BEC.

# CHAPTER FOUR

# AMPLIFICATION OF AN ISOLATED LOW-FREQUENCY MODE VIA INTERACTION WITH RAPIDLY COOLING MAGNON GAS

This chapter describes the process of coherent thermodynamic amplification of the isolated low-frequency mode via its interaction with a hot magnon gas undergoing rapid cooling. One of the features of rapidly cooling magnon gas is that its chemical potential increases (up to minimum energy of spectrum of magnons)[27], thus, providing means for accumulation of magnons at the bottom of the spectrum and subsequent Bose-Einstein condensation of magnons. However, the increase of chemical potential above the energy level of an isolated low-frequency mode (ILFM) also creates thermodynamic conditions stimulating scattering of magnons from the magnon gas into ILFM. This way one can achieve coherent amplification of an ILFM using incoherent thermal pumping of magnons by simply heating the sample.

To prove that amplification obtained is indeed coherent, the kinetic 4-wave equations have been derived with the consideration of magnon modes being coherent coherent, which corresponds to the average amplitude over ensemble of magnons in the mode having non-zero value. This also helps to account for the fact that ILFM has frequency below the minimum frequency of propagating spin waves and, therefore, has to be coherent mode rather than incoherent ensemble of many magnons corresponding to spin waves having the same frequency and different oscillation phases.

The results discussed in this chapter were previously presented in conference presentations [6], [7], [8], [9], [10], [11], [12], [13], [14].

## 4.1 Mechanism of interaction between magnon gas and an isolated mode

As a medium where a magnon gas and an ILFM coexist, a sample made of Yttrium Iron Garnet (YIG) is considered. To allow existence of an ILFM, the sample must have specific geometry (for example, a gyrotropic mode in nanodisk) and/or have other required conditions satisfied (for example, a nonlinear bullet mode). The thermal magnons can be considered as a magnon gas of certain chemical potential $\mu$ and temperature $T$. Magnons have a continuous spectrum with the minimum energy $\hbar\omega_{\text{min}}$, where $\hbar$ is the reduced Planck constant, $\omega_{\text{min}} = 2\pi f_{\text{min}}$, and $f_{\text{min}}$ is the minimum frequency of the magnon spectrum.

At equilibrium the magnon gas and the ILFM barely interact, the magnon gas has zero chemical potential ($\mu = 0$) and its temperature $T$ is equal to the temperature of the lattice $T_l$. In this case the isolated mode will demonstrate typical behavior and decay over time due to damping. The plot of magnon energy versus corresponding magnon mode population at equilibrium is depicted on Fig. 4.1 by a solid blue line.

If one heats up the sample to the heating temperature $T_h$, the magnons gas will eventually reach equilibrium with the same conditions for the chemical potential ($\mu = 0$) and the temperature ($T = T_l$), but the amount of thermal magnons will increase along with the temperature of the lattice. Essentially, this way magnons are added to the gas that would otherwise be considered as non-equilibrium ones.

During the process of rapid cooling two things happen. First, the temperature of the lattice $T_l$ rapidly drops to the cooling temperature $T_c$, which, usually, is the same temeparture as the one before heating of the sample. Second, the thermal magnons, created due to heating, become non-equilibrium and, thus, start actively interacting with the lattice and other magnons in the process of thermalization. It should be noted that high-frequency magnons interact with lattice faster than the low-frequency ones. This, together with the long magnon lifetime in YIG (around $21 \pm 4$ ns according to [27] leads to accumulation of magnons at the bottom of the spectrum. The plot of magnon energy versus magnon population in this case is shown on Fig. 4.1 by a solid red line. In terms of thermodynamics, this leads to creation of non-equilibrium state of the magnon gas with

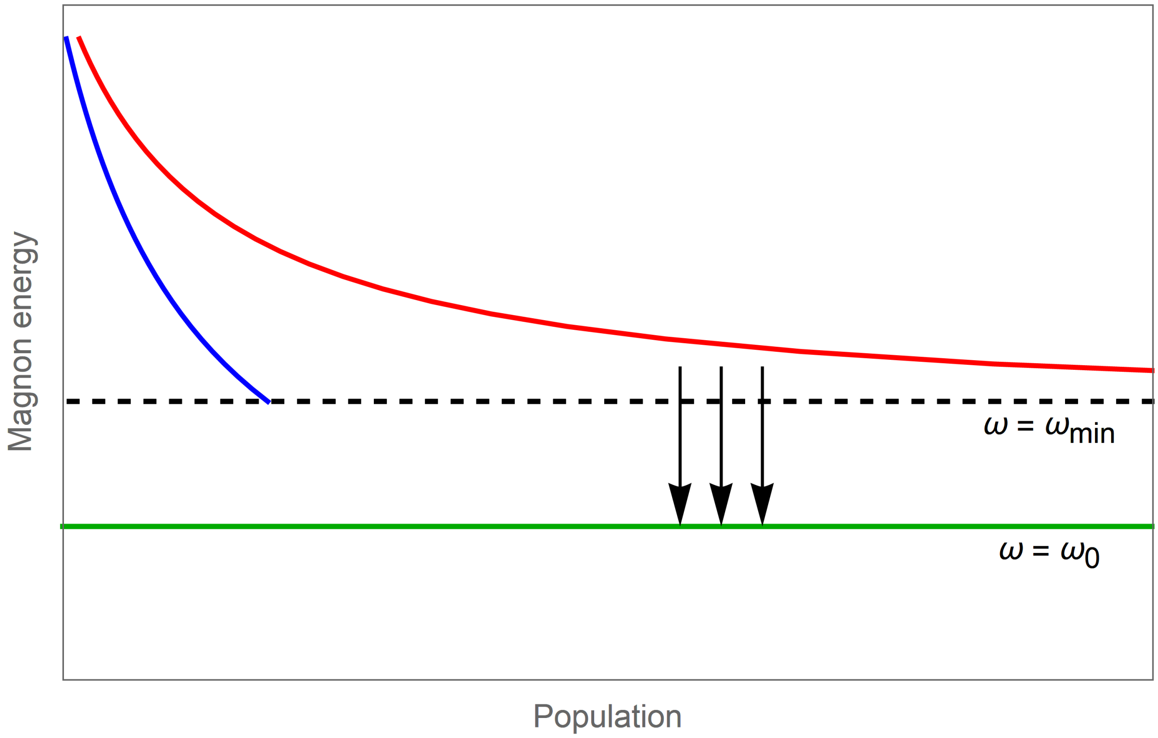


Figure 4.1: Magnon energy vs magnon mode population plotted for the cases of equilibrium ($\mu = 0$) (blue solid line), and nonzero chemical potential ($\mu > 0$) of the magnon gas (red solid line). The increase of chemical potential leads to accumulation of magnons at the bottom of the magnon spectrum and creates condition for scattering of magnons (depicted by pointing down arrows) into the isolated low-frequency mode (ILFM). The black dashed line marks the minimum energy $\hbar\omega_{min}$ of the magnon spectrum and the dark-green line marks the magnon energy of an isolated low-frequency mode.

non-zero chemical potential. The increase of the chemical potential above the magnon energy of the isolated low-frequency mode stimulates scattering of magnons from the magnons gas into the isolated mode. This can be viewed as the thermodynamic analog of a laser with inversely populated energy levels in atoms of the active environment.

## 4.2 Theoretical description

The interaction between a magnon gas and an isolated low-frequency mode can be described with a Hamiltonian that accounts for 4-magnon interactions:

$$\hat{H} = \sum_k \hbar\omega_k c_k^+ c_k + \frac{1}{4}\sum_{1234} T_{1234} c_1^+ c_2^+ c_3 c_4, \tag{4.1}$$

where $\hbar$ is the reduced Planck constant, $\omega_k$ is the frequency of the $k$-th magnon mode, $T_{1234}$ are the nonlinear interaction factors, $c_k \equiv \hat{c}_k$ and $c_k^+ \equiv \hat{c}_k^+$ are the creation and annihilation operators for the $k$-th magnon mode (here and below in the paper, hats are omitted for convenience). It should be noted, that Hamiltonian (4.1) does not distinguish between the modes corresponding to propagating spin waves and the isolated low-frequency mode.

In general, the change of the magnon mode populations can be described using 4-wave kinetic equation. However, the standard kinetic equation is derived assuming that magnons are incoherent. Therefore, the standard approach is only suitable for description of a gas of thermal magnons. The isolated low-frequency mode, on the other hand, has nonzero average amplitude and consists of coherent magnons. Thus, in general, one needs to consider each magnon modes as a mixture of an incoherent (thermal) and coherent modes. Such generalized description of a magnon mode is an analogue to a displaced thermal state.

### 4.2.1 Equations accounting for coherency of magnon modes

The derivation starts with writing down the Hamiltonian operator $\hat{H}$ considering 4-wave interaction:

$$\hat{H} = \sum_k \hbar\omega_k c_k^+ c_k + \frac{1}{4}\sum_{1234} T_{1234} c_1^+ c_2^+ c_3 c_4, \tag{4.2}$$

where $\hbar$ is the reduced Planck constant, $\omega_k$ is the frequency of the k-th magnon mode, $c_k \equiv \hat{c}_k$ and $c_k^+ \equiv \hat{c}_k^+$ are the creation and annihilation operators for the k-th magnon mode (hats are omitted for convenience).

Here a genral case if considered, when a magnon mode may have both coherent and non-coherent properties. Coherent properties correspond to excited magnon modes, for example, isolated low-frequency modes, while non-coherent properties correspond to thermal magnons having random phases of spin-waves in the ensemble. A presence of coherence also leads to non-zero value of an amplitude averaged over ensemble. Thus, operators $c_k$ and $c_k^+$, in general, describe a displaced thermal state and have the next properties:

$$\langle c_k \rangle = a_k, \tag{4.3}$$

$$\left\langle c_k^+ c_k \right\rangle = n_k + |a_k|^2, \tag{4.4}$$

where $\langle \ldots \rangle$ denotes averaging over ensemble of spin waves, $a_k = a_{0,k} e^{-i\omega_k t}$ is the average value of spin-wave amplitude over ensemble and describes coherency of the magnon mode, $\left\langle c_k^+ c_k \right\rangle$ is the total population of magnons due to non-coherent part $n_k$ (corresponds to a well know population number for magnons) and coherent part $|a_k|^2$ (appears due to non-zero average amplitude over ensemble).

Since magnons - quasi-particles of spin waves - are bosons, operators $c_k$ and $c_k^+$ inherit commutation properties of bosonic operators:

$$\left[c_j, c_k^+\right] = \Delta_{j,k} \qquad \left[c_j, c_k\right] = 0 \qquad \left[c_j^+, c_k^+\right] = 0 \tag{4.5}$$

$$c_j c_k^+ = c_k^+ c_j + \Delta_{j,k} \tag{4.6}$$

where $\Delta_{j,k}$ is the Kronecker delta (Kronecker symbol).

Usually 4-wave kinetic equation is the equation of motion for a population number $n_k = \left\langle \hat{b}_k^* \hat{b}_k \right\rangle$, where $\hat{b}_k^*$ and $\hat{b}_k$ are operators of annihilation and creation for completely non-coherent thermal magnons. In the case of completely incoherent spin waves one can not get an equation of motion, for example, for an average complex amplitude $\langle c_k \rangle$, because its average over ensemble (all possible magnons of specific frequency) is zero. However, in the presence of coherency, an average of ensemble value $a_k$ of the magnon mode $c_k$ is non-zero. Thus, in general case one can derive not only equation of motion for population number $n_k$, but the one for an average complex amplitude $a_k = \langle c_k \rangle$ as well. The end goal is to derive two kinetic equations, one for the average amplitude $a_k$ and another one for the population number $n_k$. One should also take into account, that $n_k$ is not completely independent of $a_k$, and the relation between them follows from Eq. (4.4)

$$n_k = \left\langle c_k^+ c_k \right\rangle - |a_k|^2 , \tag{4.7}$$

which means that before deriving equation of motion for $n_k$ one should first derive equations for $a_k$ and $\left\langle c_k^+ c_k \right\rangle$.

To derive the quantum 4-wave kinetic equations with consideration of coherent components of the interacting magnons one needs to write down equations of motion for the operators $c_k$ and $c_k^+ c_k$, which is only possible in the Heisenberg picture. Considering, that in the Schrodinger picture $c_k$ corresponds to the time-independent complex amplitude of a magnon mode, and $c_k^+ c_k$ corresponds to the total number of magnons in a specific magnon mode, we can use Heisenberg equations of motion:

$$i\hbar \frac{d}{dt} c_k = \left[ c_k, \hat{H} \right] . \tag{4.8}$$

$$i\hbar \frac{d}{dt} \left( c_k^+ c_k \right) = \left[ c_k^+ c_k, \hat{H} \right] \tag{4.9}$$

After expanding the commutator in the right-hand side of Eqs. (4.8) and (4.9), rewriting products of operators in the normal order and simplifying the obtained expressions we get basic equations of motion:

$$i\hbar\frac{d}{dt}c_k = \hbar\omega_k c_k + \frac{1}{2}\sum_{123} T_{k123}c_1^+ c_2 c_3. \tag{4.10}$$

$$i\hbar\frac{d}{dt}\left(c_k^+ c_k\right) = \frac{1}{2}\sum_{123}\left(T_{k123}c_k^+ c_1^+ c_2 c_3 - T_{k123}^+ c_2^+ c_3^+ c_1 c_k\right) \tag{4.11}$$

The Eq. (4.10) looks exactly like the one for the non-coherent magnons, because it does not specify properties of operators $c_k$ and $c_k^+$ related to coherency of spin waves. The Eq. (4.11) has a bit different form than typical equation for $n_k$ due to not being averaged over ensemble yet.

The next step is to average Eqs. (4.10) and (4.11) over ensemble of spin waves:

$$i\hbar\frac{d}{dt}\langle c_k\rangle = \hbar\omega_k\langle c_k\rangle + \frac{1}{2}\sum_{123} T_{k123}\left\langle c_1^+ c_2 c_3\right\rangle, \tag{4.12}$$

$$i\hbar\frac{d}{dt}\left\langle c_k^+ c_k\right\rangle = \mathrm{Im}\sum_{123} T_{k123}\left\langle c_k^+ c_1^+ c_2 c_3\right\rangle, \tag{4.13}$$

where it is considered that $T_{k123}$ and $\langle\ldots\rangle$ are complex numbers. Now Eq. (4.13) looks similar to the equation for $n_k$ in the case of incoherent magnons, again, because it does not consider properties of operators $c_k^+$ and $c_k$ explicitly. Before taking another step in derivation, it should be considered explicitly that $\langle c_k\rangle = a_k$ and denote the total population number of magnons $\left\langle c_k^+ c_k\right\rangle = m_k = n_k + |a_k|^2$. After this, Eqs. (4.12) and (4.13) transform into

$$i\hbar\frac{d}{dt}a_k = \hbar\omega_k a_k + \frac{1}{2}\sum_{123} T_{k123}\left\langle c_1^+ c_2 c_3\right\rangle, \tag{4.14}$$

$$i\hbar\frac{d}{dt}m_k = \mathrm{Im}\sum_{123} T_{k123}\left\langle c_k^+ c_1^+ c_2 c_3\right\rangle, \tag{4.15}$$

To continue derivation we use perturbation theory using interaction factors $T_{jklm}$ as a small parameter. Therefore, Eqs. (4.14) and (4.15) are essentially first-order equations of motion for $a_k$ and $m_k$. Zeroth-order equations ($T_{jklm} = 0$) correspond to non-interacting magnon modes, when the total population number $m_k$ for each mode is constant and the average complex amplitude $a_k$ rotates with the correspondent frequency $\omega_k$.

The first-order equations can be written as

$$\begin{aligned} i\hbar\frac{d}{dt}a_k &= \hbar\omega_k a_k + \sum_{12} T_{k11k} n_1 a_k \\ &= \hbar\omega_k a_k + \sum_{1} S_{k1} a_k \end{aligned} \tag{4.16}$$

$$\begin{aligned} i\hbar\frac{d}{dt}m_k &= 2i\mathrm{Im}\sum_{1} T_{k11k} n_k n_1 \\ &= 2i\mathrm{Im}\sum_{1} Q_{k1} \end{aligned} \tag{4.17}$$

Considering properties of tensor $T$, both $S$ and $Q$ are Hermitian tensors with nonzero nondiagonal elements. The interactions described by them do not change the number of magnons of modes $c_k$ and $c_1$, for example, because it is essentially scattering of magnons into themselves. What they actually describe is the modification of the mode profiles. Using a specific transformation tensors, $S$ and $Q$ can be diagonalized making non-zero components vanish, therefore, making their contribution irrelevant in terms of the effects we are interested in.

The next step is to derive second-order equations. For this we define first-order corrections $J_{123}$ and $G_{k123}$:

$$J_{123} = \left\langle c_1^+ c_2 c_3 \right\rangle \tag{4.18}$$

$$G_{k123} = \left\langle c_k^+ c_1^+ c_2 c_3 \right\rangle, \tag{4.19}$$

which are to be substituted later into Eqs. (4.14) and (4.15), respectively, to obtain equation of motion to the second order in $T_{jklm}$ describing all the nonlinear properties of magnons.

First-order corrections are solutions of corresponding equations of motion, which can be found by simply taking derivatives of Eqs. (4.18) and (4.19):

$$i\hbar\frac{d}{dt}J_{123} = i\hbar\frac{d}{dt}\left\langle c_1^+ c_2 c_3\right\rangle, \tag{4.20}$$

$$i\hbar\frac{d}{dt}G_{k123} = i\hbar\frac{d}{dt}\left\langle c_k^+ c_1^+ c_2 c_3\right\rangle. \tag{4.21}$$

After expanding the derivatives on the right hand side of Eqs. (4.20) and (4.21) and simplifying the result as much as possible we get two equations of motion for the first-order corrections $J_{123}$ and $G_{k123}$:

$$i\hbar\frac{d}{dt}J_{123} - \hbar\left(\omega_2 + \omega_3 - \omega_1\right)J_{123} = A_{123}, \tag{4.22}$$

$$i\hbar\frac{d}{dt}G_{k123} - \hbar\left(\omega_2 + \omega_3 - \omega_k - \omega_1\right)G_{k123} = B_{k123}, \tag{4.23}$$

where

$$A_{123} = \sum_j T^+_{j123}\left[n_1\left(n_2 + n_3 + 1\right) - n_2 n_3\right] a_j, \tag{4.24}$$

$$\begin{aligned} B_{k123} = {} & T^+_{k123}(n_k n_1 n_3 - n_1 n_2 n_3 - n_k n_2 n_3 - n_2 n_3) + \\ & + \sum_j T^+_{j123}\left((n_k n_1 n_2 + (n_1 n_3 + n_1 n_2 - n_2 n_3) a_k^+ a_j\right) + \\ & + \sum_l T^+_{kl23}\left(n_k n_3 + n_k n_2 - n_2 n_3\right) a_1^+ a_l + \\ & + \sum_y T^+_{k1y3}\left(n_k n_1 - n_3 n_1 - n_k n_3 - n_3\right) a_y^+ a_2 + \\ & + \sum_z T^+_{k12z}\left(n_k n_1 - n_2 n_1 - n_k n_2 - n_2\right) a_z^+ a_3 \end{aligned} \tag{4.25}$$

It should be noted, that the average value $a_k$ is considered to be small since it is assumed that the presence of the gyrotropic mode does not influence the gas of thermal magnons significantly For this reason only terms up to the first order in $a_k$ are kept in Eq. (4.24) and terms up to the second order in $a_k$ in Eq. (4.25).

With consideration of dependence of $a_j$ on time ($a_j = a_j(t) = a_{0,j}e^{-i\omega_j t}$), the solutions to the Eqs. (4.20) and (4.21) are:

$$J_{123} = C_J \exp\left[-i\left(\omega_2+\omega_3-\omega_1\right)t\right] - \sum_j \frac{A_{j123}}{\hbar\left(\omega_2+\omega_3-\omega_j-\omega_1\right)}, \tag{4.26}$$

$$G_{k123} = C_G \exp\left[-i\left(\omega_2+\omega_3-\omega_k-\omega_1\right)t\right] - \frac{B_{k123}}{\hbar\left(\omega_2+\omega_3-\omega_k-\omega_1\right)}, \tag{4.27}$$

where $A_{j123}$ is a single term in Eq. (4.24), i.e. $A_{123} = \sum_j A_{j123}$.

Further simplification of Eqs. (4.26) and (4.27) is required. For this. the interaction $T^+_{jklm}$ in $A_{123}$ and $B_{k123}$is is included adiabatically slowly, and at $t \to -\infty$ the interaction between magons is assumed to be absent. To account for this we add a factor of $\exp(\Gamma t)$ with $\Gamma \ll 1$ to the right-hand sides of Eqs.(4.20) and (4.21):

$$i\hbar\frac{d}{dt}J_{123} - \hbar\left(\omega_2+\omega_3-\omega_1\right)J_{123} = A_{123}\exp(\Gamma t), \tag{4.28}$$

$$i\hbar\frac{d}{dt}G_{k123} - \hbar\left(\omega_2+\omega_3-\omega_k-\omega_1\right)G_{k123} = B_{k123}\exp(\Gamma t). \tag{4.29}$$

The influence of this step on the solutions (4.26) and (4.27) we obtained before is limited to the replacement

$$\omega_j \to \omega_j + i\Gamma. \tag{4.30}$$

Then, considering the discussion above, the solutions to Eqs. (4.20) and (4.21) take the form

$$J_{123} = C_J \exp\left[-i\left(\omega_2+\omega_3-\omega_1\right)t\right] - \sum_j \frac{A_{j123}}{\hbar\left(\omega_2+\omega_3-\omega_j-\omega_1-i\Gamma\right)}, \tag{4.31}$$

$$G_{k123} = C_G \exp\left[-i\left(\omega_2+\omega_3-\omega_k-\omega_1\right)t\right] - \frac{B_{k123}}{\hbar\left(\omega_2+\omega_3-\omega_k-\omega_1-i\Gamma\right)}. \tag{4.32}$$

To further simplify the solution we introduce notation

$$\omega = \omega_2+\omega_3-\omega_1-\omega_j \tag{4.33}$$

and use properties of complex numbers:

$$\frac{1}{\omega-i\Gamma} = \frac{\omega}{\omega^2+\Gamma^2} + \frac{i\Gamma}{\omega^2+\Gamma^2}. \tag{4.34}$$

The expression in Eq. (4.31) can be simplifies considering that $\Gamma \ll \omega$:

$$\frac{1}{\omega-i\Gamma} \approx \frac{1}{\omega} + \frac{i\Gamma}{\omega^2+\Gamma^2}. \tag{4.35}$$

The fist term in Eq. (4.35) can not be simplified further, while the second one can be simplified using an integral relation due to $\Gamma$ being a very small damping ($\Gamma \ll 1$):

$$\int_{-\infty}^{\infty} \frac{\Gamma}{\omega^2+\Gamma^2} d\omega = \int_{-\infty}^{\infty} \pi\delta(\omega) d\omega = \pi, \tag{4.36}$$

which makes the two expressions equivalent in integral way:

$$\frac{\Gamma}{\omega^2+\Gamma^2} \equiv \pi\delta(\omega), \tag{4.37}$$

meaning

$$\frac{1}{\omega-i\Gamma} = \frac{1}{\omega} + i\pi\delta(\omega) \tag{4.38}$$

Using Eq. (4.38), the solutions (4.31) and (4.32) are transformed for the last time:

$$\begin{aligned} J_{123} =& C_J \exp\left[-i\left(\omega_2+\omega_3-\omega_1\right)t\right] - \sum_j \frac{A_{j123}}{\hbar(\omega_2+\omega_3-\omega_j-\omega_1)} \\ & - i\pi \sum_j A_{j123}\delta(\omega_2+\omega_3-\omega_j-\omega_1), \end{aligned} \tag{4.39}$$

$$\begin{aligned} G_{k123} = & C_G \exp\left[-i\left(\omega_2+\omega_3-\omega_k-\omega_1\right)t\right] - \frac{B_{k123}}{\hbar(\omega_2+\omega_3-\omega_k-\omega_1)} \\ & - i\pi \tilde{B}_{k123}\delta(\omega_2+\omega_3-\omega_k-\omega_1), \end{aligned} \tag{4.40}$$

where

$$A_{j123} = T^{+}_{j123}\left[n_1(n_2+n_3+1)-n_2n_3\right]a_j, \tag{4.41}$$

$$\begin{aligned} \tilde{B}_{k123} = T^{+}_{k123}\Big[ & ((n_k+1)(n_1+1)n_2n_3 - n_kn_1(n_2+1)(n_3+1)) \\ & + (-n_2n_3+n_1n_3+n_1n_2+n-1)\,|a_k|^2 \\ & + (-n_2n_3+n_kn_3+n_kn_2+n_k)\,|a_1|^2 \\ & + (-n_3n_1-n_3-n_kn_3+n_kn_1)\,|a_2|^2 \\ & + (-n_2n_1-n_2-n_kn_2+n_kn_1)\,|a_3|^2\Big]. \end{aligned} \tag{4.42}$$

Equations (4.41) and (4.42) can be further simplified by using additional notation:

$$A_{j123} = T^{+}_{j123}g_{123}a_j, \tag{4.43}$$

$$\tilde{B}_{k123} = T^{+}_{k123}\left(f_{k123} + |a_k|^2 g_{123} + |a_1|^2 g_{k23} - |a_2|^2 g_{3k1} - |a_3|^2 g_{2k1}\right), \tag{4.44}$$

where

$$f_{k123} = (n_k+1)(n_1+1)n_2n_3 - n_kn_1(n_2+1)(n_3+1) \tag{4.45}$$

$$g_{jly} = n_ln_y - n_j(n_l+n_y+1) \tag{4.46}$$

Using notation from Eqs (4.43)-(4.46), solutions (4.39) and (4.40) can be written as

$$
\begin{aligned}
J_{123} = C_J \exp\left(-i\left(\omega_2+\omega_3-\omega_1\right)t\right) - \sum_j \frac{T^{+}_{j123} g_{123} a_j}{\hbar(\omega_2+\omega_3-\omega_j-\omega_1)} \\
- i\pi \sum_j T^{+}_{j123} g_{123} a_j \delta(\omega_2+\omega_3-\omega_j-\omega_1)
\end{aligned}
\tag{4.47}
$$

$$
\begin{aligned}
G_{k123} = C_G \exp\left[-i\left(\omega_2+\omega_3-\omega_k-\omega_1\right)t\right] - \frac{B_{k123}}{\hbar(\omega_2+\omega_3-\omega_k-\omega_1)} \\
- i\pi T^{+}_{k123} \left(f_{k123} + |a_k|^2 g_{123} + |a_1|^2 g_{k23} - |a_2|^2 g_{3k1} - |a_3|^2 g_{2k1}\right),
\end{aligned}
\tag{4.48}
$$

Next, the substitution of Eqs. (4.50) and (4.51) into Eqs. (4.14) and (4.15), respectively, yields

$$
\begin{aligned}
i\hbar \frac{d}{dt} a_k = \hbar\omega_k a_k + \frac{1}{2}\sum_{123} T_{k123} C_J \exp\left(-i(\omega_2+\omega_3-\omega_1)t\right) \\
- \frac{1}{2}\sum_{j123} \frac{T_{k123} T^{+}_{j123} g_{123} a_j}{\hbar(\omega_2+\omega_3-\omega_j-\omega_1)} \\
- i\frac{\pi}{2} \sum_{j123} T_{k123} T^{+}_{j123} g_{123} a_j \delta(\omega_2+\omega_3-\omega_j-\omega_1)
\end{aligned}
\tag{4.49}
$$

$$
\begin{aligned}
i\hbar \frac{d}{dt} m_k = i\mathrm{Im}\Bigg[\sum_{123} T_{k123} C_G \exp\left[-i\left(\omega_2+\omega_3-\omega_k-\omega_1\right)t\right] - \sum_{123} \frac{B_{k123}}{\hbar(\omega_2+\omega_3-\omega_k-\omega_1)} \\
- i\pi \sum_{123} |T_{k123}|^2 \left(f_{k123} + |a_k|^2 g_{123} + |a_1|^2 g_{k23} - |a_2|^2 g_{3k1} - |a_3|^2 g_{2k1}\right) \times \\
\times \delta(\omega_2+\omega_2-\omega_k-\omega_1)\Bigg],
\end{aligned}
\tag{4.50}
$$

In Eq. (4.49) the second and the third terms must be considered as a part of nonlinear frequency shift. Therefore, one needs to consider their ratio to the amplitude $a_k$.

Since $C_J$ is arbitrary constant, we can set it to $a_k$, then

$$\frac{C_J}{a_k}\sum_{123} T_{k123}\exp\left(-i(\omega_2+\omega_3-\omega_1)t\right) = \sum_{123} T_{k123}\exp\left(-i(\omega_2+\omega_3-\omega_k-\omega_1)t\right), \quad (4.51)$$

which is oscillating term unless $\omega_2+\omega_3=\omega_k+\omega_1$:

$$\frac{C_J}{a_k}\sum_{123} T_{k123}\exp\left(-i(\omega_2+\omega_3-\omega_1)t\right) = \sum_{123} T_{k123}\Delta_{(\omega_2+\omega_3,\omega_k+\omega_1)} \quad (4.52)$$

The third term in Eq. (4.49) after division by $a_k$ will have a factor of $\exp\left(-i(\omega_j-\omega_k)t\right)$ and the only non-oscillating terms would have $\omega_j=\omega_k$:

$$\frac{1}{2}\sum_{j123}\frac{T_{k123}T^{+}_{j123}g_{123}}{\hbar(\omega_2+\omega_3-\omega_j-\omega_1)}\frac{a_j}{a_k} = \frac{1}{2}\sum_{j123}\frac{T_{k123}T^{+}_{j123}g_{123}}{\hbar(\omega_2+\omega_3-\omega_j-\omega_1)}\Delta_{\omega_j,\omega_k} \quad (4.53)$$

This allows us to introduce the frequency $\omega'_k$ with consideration of nonlinear shift:

$$\omega'_k = \omega_k + \frac{1}{2}\Omega_k, \quad (4.54)$$

where $\Omega_k$ is:

$$\Omega_k = \sum_{123} T_{k123}\Delta_{(\omega_2+\omega_3,\omega_k+\omega_1)} - \sum_{j123}\frac{T_{k123}T^{+}_{j123}g_{123}}{\hbar(\omega_2+\omega_3-\omega_j-\omega_1)}\Delta_{\omega_j,\omega_k} \quad (4.55)$$

It should be noted, that the first term in $\Omega_k$ disappears if $C_J=0$.

In Eq. (4.50) only the first and the third terms contain imaginary part and, therefore, contribute to the change in $m_k$:

$$\begin{aligned} i\hbar\frac{d}{dt}m_k = i\mathrm{Im}\left[\sum_{123} T_{k123}C_G\exp\left[-i\left(\omega_2+\omega_3-\omega_k-\omega_1\right)t\right]\right] \\ -\pi\sum_{123}|T_{k123}|^2\left(f_{k123}+|a_k|^2g_{123}+|a_1|^2g_{k23}-|a_2|^2g_{3k1}-|a_3|^2g_{2k1}\right)\times \\ \times\,\delta(\omega_2+\omega_3-\omega_k-\omega_1), \end{aligned} \quad (4.56)$$

From Eq. (4.53) it is seen that $C_G$ describes the change of total population number $m_k$ when the system is at equilibrium, which contradicts itself, therefore $C_G = 0$.

Now, the equations of motion for the average amplitude $a_k$ and the total population number $m_k$ can be written down:

$$\frac{da_k}{dt} = -i\omega_k' a_k + \frac{\pi}{2\hbar^2}\sum_{123} |T_{k123}|^2 g_{123} a_k, \tag{4.57}$$

$$\begin{aligned}\frac{dm_k}{dt} =& \frac{\pi}{\hbar^2}\sum_{123} |T_{k123}|^2 \left(f_{k123} + |a_k|^2 g_{123} + |a_1|^2 g_{k23} - |a_2|^2 g_{3k1} - |a_3|^2 g_{2k1}\right)\times \\ &\times \delta(\omega_2 + \omega_3 - \omega_k - \omega_1).\end{aligned} \tag{4.58}$$

Using kinetic equations for the average value $a_k$ and total population number $m_k$, the kinetic equation for the population number $n_k$ is derived:

$$\begin{aligned}\frac{dn_k}{dt} =& \frac{\pi}{\hbar^2}\sum_{k123} |T_{k123}|^2 \left(f_{k123} + |a_1|^2 g_{k23} - |a_2|^2 g_{3k1} - |a_3|^2 g_{2k1}\right)\times \\ &\times \delta(\omega_2 + \omega_3 - \omega_k - \omega_1),\end{aligned} \tag{4.59}$$

where the notation used is the same as before. This completes the system of kinetic equations and the notations used:

$$\frac{da_k}{dt} = -i\omega_k' a_k + \frac{\pi}{2\hbar^2}\sum_{123} |T_{k123}|^2 a_k g_{123} \times \delta(\omega_2 + \omega_3 - \omega_k - \omega_1), \tag{4.60}$$

$$\begin{aligned}\frac{dn_k}{dt} =& \frac{\pi}{\hbar^2}\sum_{123} |T_{k123}|^2 \left(f_{k123} + |a_1|^2 g_{k23} - |a_2|^2 g_{3k1} - |a_3|^2 g_{2k1}\right)\times \\ &\times \delta(\omega_2 + \omega_3 - \omega_k - \omega_1),\end{aligned} \tag{4.61}$$

$$\begin{aligned}\frac{dm_k}{dt} =& \frac{\pi}{\hbar^2}\sum_{123} |T_{k123}|^2 \left(f_{k123} + |a_k|^2 g_{123} + |a_1|^2 g_{k23} - |a_2|^2 g_{3k1} - |a_3|^2 g_{2k1}\right)\times \\ &\times \delta(\omega_2 + \omega_3 - \omega_k - \omega_1).\end{aligned} \tag{4.62}$$

$$\omega'_k = \omega_k + \frac{1}{2}\Omega_k, \tag{4.63}$$

$$\Omega_k = \sum_{123} T_{k123}\Delta_{(\omega_2+\omega_3,\omega_k+\omega_1)} - \sum_{j123} \frac{T_{k123}T^{+}_{j123}g_{123}}{\hbar(\omega_2+\omega_3-\omega_j-\omega_1)}\Delta_{\omega_j,\omega_k} \tag{4.64}$$

$$g_{jly} = n_l n_y - n_j(n_l + n_y + 1) \tag{4.65}$$

$$f_{k123} = (n_k+1)(n_1+1)n_2 n_3 - n_k n_1 (n_2+1)(n_3+1) \tag{4.66}$$

It should be noted, that in the case of completely incoherent magnons ($a_0 = 0$, $a_j = 0$) Eq.(4.61) transforms into a standard 4-wave kinetic equation:

$$\frac{dn_0}{dt} = \frac{\pi}{\hbar^2}\sum_{123} |T_{0123}|^2 f_{0123}, \tag{4.67}$$

while Eq. (4.60) can be ignored completely. Hence, as expected, the equations derived are backward compatible with the standard 4-wave kinetic equation.

4.2.2 Adaptation of general theory to the considered case

The next step is to adapt the theory developed in the previous subsection to the specific case: interaction of rapidly cooling magnon gas with ILFM.

In the example considered, an isolated low-frequency mode interacts with a gas of thermal (incoherent) magnons. The low-frequency mode is called isolated because it is located below the spectrum of propagating spin waves, sometimes with quite significant gap. Such modes are coherent and do not have a defined wavevector, hence, momentum does not have to conserve in the interaction with other magnons.

The process of such interaction between ILFM and a magnon gas can be considered as interaction between fully coherent magnon mode $c_k$ and fully non-coherent modes $c_1$, $c_2$ and $c_3$. The frequency of the coherent mode $\omega_k$ is considered to be already nonlinearly shifted, because the frequencies observed in experiment are the ones already affected by nonlinear shift. In this case, the equations will be simplified to

$$\frac{da_0}{dt} = -i\omega_0 a_0 + \frac{\pi}{2\hbar^2}\sum_{123} |T_{0123}|^2 a_0 g_{123} \times \delta(\omega_2 + \omega_3 - \omega_0 - \omega_1), \tag{4.68}$$

$$\frac{dn_0}{dt} = \frac{\pi}{\hbar^2}\sum_{123} |T_{0123}|^2 f_{0123} \times \delta(\omega_2 + \omega_3 - \omega_0 - \omega_1), \tag{4.69}$$

$$\frac{dm_0}{dt} = \frac{\pi}{\hbar^2}\sum_{123} |T_{0123}|^2 \left(f_{0123} + |a_0|^2 g_{123}\right) \times \delta(\omega_2 + \omega_3 - \omega_0 - \omega_1). \tag{4.70}$$

$$g_{jly} = n_l n_y - n_j(n_l + n_y + 1) \tag{4.71}$$

$$f_{k123} = (n_k + 1)(n_1 + 1)n_2 n_3 - n_k n_1 (n_2 + 1)(n_3 + 1) \tag{4.72}$$

With consideration of the notation used, the equation for population number $n_0$ of an ILFM looks the same way as for interaction of incoherent magnon modes only, while the total population number $m_0$ gets amplified with consideration of both coherency and incoherency.It should be noted that kinetic equations for incoherent magnons interacting with ILFM will include terms proportional to coherency of the ILFM.

From the equation for average amplitude $a_0$ one can see that the interaction between ILFM and a magnon gas may lead to amplification of the average amplitude, which is detectable in experiments. This allows to assume that amplification of an ILFM interacting with a gas of thermal magnons is the coherent one.

4.2.3 Condition for amplification of a coherent mode

To analyze amplification of the coherent magnon mode interacting with a gas of noncoherent magnons (thermal magnons), Eq. (4.60) can be rewritten as:

$$\hbar\frac{da_0}{dt} + i\hbar\omega_0' a_0 = \frac{\pi}{2\hbar}\sum_{123} |T_{0123}|^2 a_0 g_{123} \times \delta(\omega_2 + \omega_3 - \omega_0 - \omega_1). \tag{4.73}$$

It is obvious, that average amplitude $a_0$ will be amplified if the right hand side is positive:

$$\frac{\pi}{2\hbar}\sum_{123}|T_{k123}|^2 a_k g_{123} > 0. \tag{4.74}$$

One can see, that the only value that could possibly be negative is $g_{123}$, hence we analyze it.

Let us assume that the modes $c_1$, $c_2$ and $c_3$ correspond to noncoherent propagating spin waves, while the amplified mode $c_k$ is a fully coherent mode. In general, there is no simple way to describe population numbers $n_j$ in a non-equilibrium state. However, magnons in ferromagnet interact with each other faster than with phonons of the lattice. Considering a long lifetime of magnons in YIG, one can assume that interaction between magnons is much faster than with the lattice. Therefore, the gas of magnons can be considered to be in quasi-equilibrium state with certain values of chemical potential $\mu$ and effective temperature $T$ during the whole process of rapid cooling. Then, populations $n_1$, $n_2$ and $n_3$ are determined by Bose-Einstein distribution in the assumption of quasi-equilibrium magnon gas:

$$n_j = \frac{1}{\exp\left(\frac{\hbar\omega_j - \mu}{k_B T}\right) - 1} \tag{4.75}$$

where $k_B$ is the Boltzmann constant, $\mu$ and $T$ are the chemical potential and the effective temperature of the magnon gas, respectively. The quasi-equilibrium state of magnon gas also implies that we neglect the influence of the interaction between the magnon gas and the isolated low-frequency mode on the population numbers $n_j$ of magnons in the gas.

After introducing notation

$$r_j = \exp\left(\frac{\hbar\omega_j - \mu}{k_B T}\right) \tag{4.76}$$

$$n_j = \frac{1}{r_j - 1} \tag{4.77}$$

we can rewrite $g_{123}$:

$$\begin{aligned} g_{123} &= \frac{1}{(r_2-1)(r_3-1)} - \frac{1}{r_1-1}\left[\frac{r_3-1+r_2-1+(r_3-1)(r_2-1)}{(r_3-1)(r_2-1)}\right] = \\ &= \frac{r_1-1-r_3+1-r_2+1-r_2r_3+r_2+r_3-1}{(r_1-1)(r_2-1)(r_3-1)} = \\ &= \frac{r_1 - r_2r_3}{(r_1-1)(r_2-1)(r_3-1)} \end{aligned} \tag{4.78}$$

After converting values $r_j$ back to population numbers and exponents, we get inequality

$$n_1n_2n_3\left[\exp\left(\frac{\hbar\omega_1-\mu}{k_BT}\right) - \exp\left(\frac{\hbar(\omega_2+\omega_3)-2\mu}{k_BT}\right)\right] > 0, \tag{4.79}$$

which, with consideration of the energy conservation during the 4-magnon process ($\omega_k + \omega_1 = \omega_2 + \omega_3$), can be further simplified to

$$n_1n_2n_3\exp\left(\frac{\hbar\omega_1-\mu}{k_BT}\right)\left[1-\exp\left(\frac{\hbar\omega_k-\mu}{k_BT}\right)\right] > 0 \tag{4.80}$$

While analyzing Eq. (4.80) one can notice, that population numbers $n_1$, $n_2$ and $n_3$ are always positive. The sign of the factor in brackets, on the other hand, depends on the value of the chemical potential of the magnon gas $\mu$. To satisfy the inequality (4.80) one must ensure that

$$\exp\left(\frac{\hbar\omega_k - \mu}{k_b T}\right) < 1 \tag{4.81}$$

which leads us to

$$\mu > \hbar\omega_k \tag{4.82}$$

According to inequality (4.82), the coherent magnon mode will be amplified if the chemical potential of the magnon gas $\mu$ is greater than corresponding energy $\hbar\omega_k$ of the coherent mode.

In the equilibrium state chemical potential of a magnon gas is zero ($\mu = 0$), therefore, the expression in parenthesis has positive value and the nonlinear damping $\Gamma_{\mathrm{nl}}$ is positive. However, if the chemical potential exceeds the magnon energy of the isolated mode ($\mu > \hbar\omega_0$), the noninear damping becomes negative, which leads to amplification of an isolated low-frequency mode. Since the amplification condition is derived from the equation for the average amplitude of ILFM, the resulting amplification of an isolated low-frequency mode will be coherent. Also, the condition for coherent amplification $\mu > \hbar\omega_0$ does not depend on population numbers $n_j$ of the thermal magnons interacting with the isolated low-frequency mode. This makes the amplification condition general and the sum over different interactions in Eq. (4.74) does not introduce any additional effects.

4.2.4 Calculation of effective parameters of magnon gas

The assumption about magnons inside magnon gas interacting with each other much faster than with lattice allows one to consider that magnon gas is in quasi-equilibrium state. This allows one to use Bose-Einstein distribution for description of populations $n_j$ of interacting magnon modes:

$$n_j = \frac{1}{\exp\left(\frac{\hbar\omega_j - \mu_{eff}}{k_B T_{eff}}\right) - 1}, \tag{4.83}$$

where $\hbar$ is the Planck constant, $\omega_j$ is the frequency of the $j$-th magnon mode, $\mu_{eff}$ and $T_{eff}$ are the effective chemical potential and the effective temperature of the magnons gas, respectively.

The process of linearization of Eq. (4.83) yields

$$\frac{1}{n} + 1 = \exp\left(\frac{\hbar\omega - \mu_{eff}}{k_B T_{eff}}\right) \tag{4.84}$$

$$\ln\left(\frac{1}{n} + 1\right) = \frac{\hbar\omega}{k_B T_{eff}} - \frac{\mu_{eff}}{k_B T_{eff}} \tag{4.85}$$

Eq. (4.85) resembles the equation of a straight line:

$$y = ax + b, \tag{4.86}$$

in which case

$$a = \frac{\hbar}{k_B T_{eff}}, \qquad b = -\frac{\mu_{eff}}{k_B T_{eff}}. \tag{4.87}$$

Using Eq. (**??**) one can easily find effective chemical potential $\mu_{eff}$ and temperature $T_{eff}$ of magnon gas from the linear fit of the simulated or experimental data points:

$$\mu_{eff} = -\hbar\frac{b}{a}, \qquad T_{eff} = \frac{ak_B}{\hbar} \tag{4.88}$$

To verify the validity of quasi-equilibrium approximation, the data obtained from numerical simulation has been analyzed. Fig. 4.2 shows time profiles of the lattice temperature used in the simulation and the population at the minimum of the magnon spectrum. The peak of the population of magnons is due to rapid cooling of the magnon gas. We then look at the validity of the assumption at different times. We do not check validity of the assumption at initial heating temperature because system is literally in equilibrium. Parameters used for the test are: simulation period of 10 ns, cooling temperature $T_\mathrm{c} = 288$ k and the heating temperature $T_\mathrm{h} = 431.4$ K, cooling time 1 ns.

On the Fig. 4.3 one can see the linearized data in the assumption of Bose-Esintein distribution. The x-intercept allows us to find the effective chemical potential $\mu_{eff}$, and the slope of the line is connected to the effective temperature of the magnon gas $T_{eff}$. As one can see, the linearized simulation data is very well fit with with a straight line, which means that the validity of the assumption on the quasi-equilibrium magnon distribution is successfully verified.

On Fig. 4.4 one can see distribution of population of magnons over frequencies for different time after the start of rapid cooling: $t_1 =$ ns, $t_2 =$ ns, and $t_3 =$ ns. Dots correspond to the simulated data and solid lines correspond to curve fits using Bose-Einstein distribution. The population profiles shown agree with the change in time of the lowest magnon mode population shown on Fig.1. By using this fitting we easily obtain time profiles of the magnon gas temperature $T_{eff}$ and its chemical potential $\mu_{eff}$. The time profiles of $T_{eff}$ and $\mu_{eff}$ are shown on Fig. 4.5. As one can see, while the temperature of the magnon gas gradually decrease in time, the chemical potential experiences increase due to rapid cooling of the magnon gas.

## 4.3 Results

The process of coherent amplification of an isolated low-frequency mode was analyzed for the case of a particular isolated low-frequency mode. Different kinds of isolated low-frequency modes (ILFM) include a gyrotropic mode [28], [29], an edge mode [30] and a nonlinear bullet mode (references). The edge mode is localized at the edge of the magnetic sample [30] while BEC of magnons is usually created in the middle of the sample, which makes the interaction between two negligible. In contrary to an edge mode, a nonlinear bullet mode can be excited in the area where BEC is created. However, a nonlinear bullet mode has strongly nonlinear damping which complicates the theoretical analysis and the search of reasonable simulation parameters. Therefore, we decided to focus on a gyrotropic mode. The gyrotropic mode has a linear damping and its power is directly related to the radius of the vortex core precession.

To demonstrate the process of coherent amplification of a gyrotropic mode, numerical simulations have been performed in Wolfram Mathematica using a model first proposed in [27]. The model was adapted to account for coherence of a gyrotropic mode as described in the previous section. An example simulation was done for the cooling temperature of $T_c = 288$ K and the heating temperature of $T_h = 431.4$ K, same as in [27]. The simulated process consists of 30 ns of heating to the temperature $T_h$ and rapid cooling of the sample down to $T_c$ in the cooling time of 1 ns. The initial populations of magnons in YIG were set using Bose-Einstein distribution with $T = T_c$ and $\mu = 0$. The gyrotropic mode, in contrary to incoherent thermal magnons, has a non-zero average amplitude $a_0$. In general, the incoherent component can be present as well, however, unlike thermal magnons the gyrotropic mode is absent at equilibrium and has to be excited in coherent way. Thus, the corresponding noncoherent population $n_0$ of the gyrotropic mode at the start of the simulation was set to 0: $n_0(t = 0) = 0$. The average amplitude of a gyrotropic mode, on the other hand, is non-zero at $t = 0$ ns (the mode is considered to be excited previously), and, on practice, depends on the radius of the vortex core precession. The radius of the vortex core precession is proportional to the power of the gyrotropic mode. It, however, would also depends on the effective mass of the vortex core which is unknown. Therefore, in simulations the average amplitude of the gyrotropic mode $a_0$ was a manually set parameter rather than a calculated one. The initial value of $a_0$ was set at the start of simulation and then the gyrotropic mode was allowed to decay in time due to its natural damping and interaction with the meagnon gas. The results of the simulation - temporal profiles of the magnon population at the spectral minimum ($\omega = \omega_{\text{min}}$) and lattice temperature - are shown on Fig. 4.6. Here we observe accumulation of low-frequency magnons in YIG due to rapid cooling of the sample.

The simulation data have been used to verify the assumption about magnon gas being in quasi-equilibrium state. The linearized population data is very well fit by a linear depedence at the frequency range from $f_{\text{min}} = 5.3$ GHz to at least 14 GHz. The reason we do not verify the requirement for very high frequencies is because the gyrotropic mode interacts mainly with magnons at the bottom of the spectrum, so the influence of high-frequency magnons is negligible. Also, during the process of rapid cooling high-frequency magnons have rather low population compared to the low-frequency ones. These factors allow us to consider the state of the magnon gas as quasi-equilibrium.

Using the linearized magnon population data we found how the chemical potential and the temperature of the magnon gas change in time. These results are shown on Fig. 4.7 (solid lines), along with the lines that mark minimum frequency of magnons in the gas and the frequency of the gyrotropic mode (dashed lines). As one can see, in a certain time interval the chemical potential of the magnon gas $\mu$ exceeds the energy of the gyrotropic mode magnons $\hbar\omega_0$. The influence of rapid cooling on the average amplitude $a_0$ of the gyrotropic mode is shown on Fig. 4.8. It is easy to notice the increase of average amplitude $a_0$ soon after the start of rapid cooling, which is expected according to amplification condition $\mu > \hbar\omega_0$ and results shown on Fig. 4.7. The amplification is a continuous process in a time interval defined by lifetime of BEC of magnons in FM sample, after which the gyrotropic mode continues its exponential decay due to natural damping.

After confirming presence of amplification we quantified the amplification effect by calculating the amplification gain as a ratio of an amplified mode amplitude to the nonamplified one. The analytical expression for the total amplification gain can be derived from (4.68) and has the form:

$$\text{Amplification} = \exp\left(-\int_0^t \left(\Gamma_{\text{nl}}^{(rc)} - \Gamma_{\text{nl}}^{(eq)}\right) dt\right) \tag{4.89}$$

where $\Gamma_{\text{nl}}^{\text{rc}}$ is the the nonlinear damping when the rapid cooling is performed and $\Gamma_{\text{nl}}^{(\text{eq})}$ is the nonlinear damping due to interaction between the isolated low frequency mode and thermal magnons at a constant temperature. The integration in Eq. (**??**) is done over the period of time during which the interaction between the gyrotropic mode and the magnons gas is considered, in this case - from the start of simulation at time $t = 0$.

The simulation starts from equilibrium state either at cooling temperature $T_c$ (to simulate the amplitude decay at equilibrium) with a 20 ns waiting time after which a 60 ns heating pulse is applied with the cut-off time (cooling time) of 1 ns. The amplification of an ILFM is a continuous process of certain duration. To account for change of average amplitude of ILFM $a_0$ during the hating phase and active interaction between magnon gas and ILFM riht after rapid cooling, the amplification factor was measured far from the moment of rapid cooling, which was ensured by the total simulation duration of 300 ns.

To evaluate the validity of the quasi-equilibrium approximation, the amplification gain has been calculated using both simulated data and Eq. (4.89). The comparison of the results obtained is depicted on Fig 4.9 as a plot of the amplification gain versus the heating temperature $T_{\text{h}}$. The amplification increases with the increase of heating temperature, which is expected as the negative damping $\Gamma_{\text{nl}}$ is proportional to populations of magnons in the gas, which increase with the increase of the heating temperature $T_{\text{h}}$. Total amplification is also increased by the increase of the time period when chemical potential exceeds the energy of the gyrotropic mode magnons. Closer to $T_{\text{h}} = 420$ K calculated data has a sign of saturation of the amplification gain. This is due to the fact that during the heating period the interaction between the magnon gas and a gyrotropic mode leads to decrease of average amplitude of the latter, which becomes quite significant at high heating temperatures. At certain heating temperature the decrease becomes comparable with the increase of average amplitude due to the amplification effect, which limits the amplification gain and leads to its decrease at further increase of heating temperature $T_{\mathrm{h}}$. Simulations performed for heating temperatures $T_{\mathrm{h}}$ above 420 K show the same effect. From Fig. 4.9 one can also see that amplification factor decreases with the decrease of heating temperature. If there is no heating pulse applied, the amplification factor is equal 1, which means absence of amplification, which is expected.

Although The values of total amplification gain found in simulated data and theory are in qualitative agreement, the discrepancy between amplification factors found by different methods increases with the increase of heating temperature $T_{\mathrm{h}}$ This is due to greater change of temperature during rapid cooling, thus, making the transition process less close to quasi-equilibrium. This also means that at very high heating temperatures $T_{\mathrm{h}}$ the assumption of quasi-equilibrium magnon gas may not be applicable.

## 4.4 Conclusion

The effect of amplification of an isolated low-frequency mode (ILFM) demonstrated here for the particular case of a gyrotropic mode with a linear damping can be generalized for for the case of arbitrary ILFM, because it will only change the damping function and influence the interaction efficiency.

The thermal coherent amplification effect described is supported by the recent experiments [31] regards the interaction of the rapidly cooling magnon gas with the nonlinear bullet mode. Indeed, depending on the temperature a magnon gas was heated to by an electric pulse passing through the sample, the bullet mode lifetime was either short or significantly prolonged.

Another interesting previously reported effect [32] is the amplification of the propagating spin wave. Although amplification of propagating spin waves is not possible in the model presented here because chemical potential of a magnon gas $\mu$ never exceeds the minimum energy of a spectrum of propagating spin waves, it still might have similar cause. It worth noting that here it is assumed that in the process of rapid cooling a magnon gas is always in quasi-equilibrium. This is not fully true as in the process of thermalization the gas is never in full equilibrium. However, the explanation of propagating spin wave amplification involves some local (in terms of energy of magnons) equilibrium leading to effective chemical potential of some parts of a magnon gas exceeding the energy level of a propagating spin wave [32].

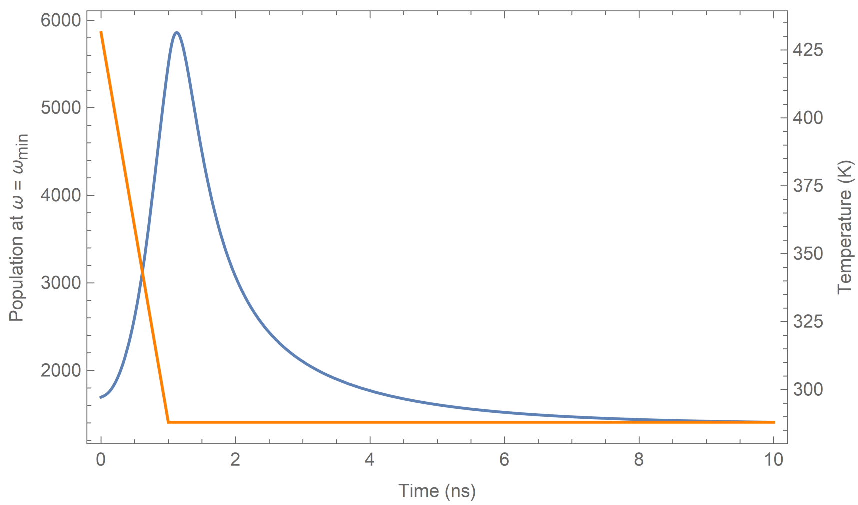


Figure 4.2: The time profile of the lattice temperature used in simulation and the population number n for the lowest magnon mode of the magnon gas.The step-like temperature dependence imitates the process of rapid cooling of the sample. Local in time increase of the magnon population illustrates the accumulation of magnkons at the bottom of the spin wave spectrum.

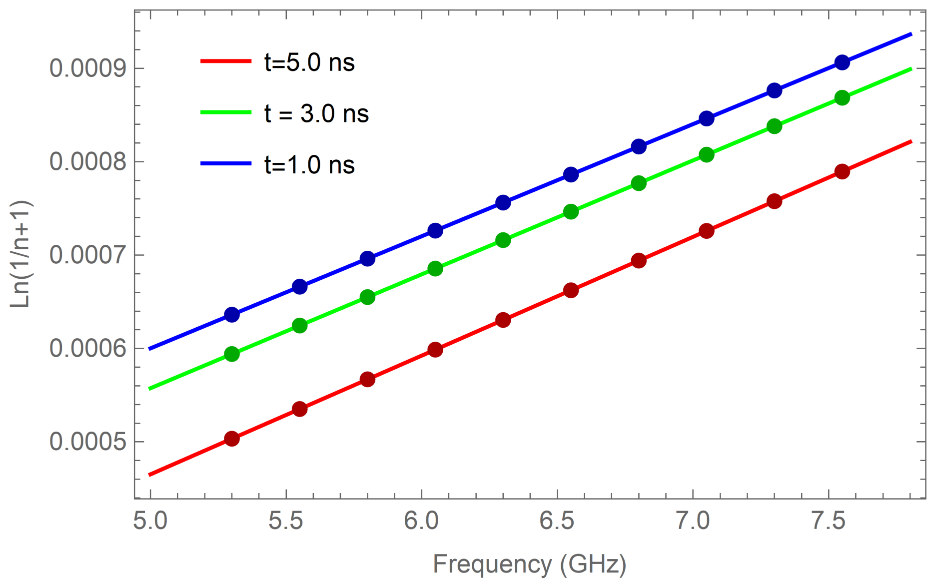


Figure 4.3: Demonstration of the fitting procedure for dependence of magnon population $n$ on the magnon frequency $f$ in the assumption of quasi-equilibrium magnon distribution for different time after the start of rapid cooling: $t_1 =$ ns, $t_2 =$ ns, and $t_3 =$ ns. Data points represent the linearized result of simulation, and the solid lines represent the linear fit of the data. The data points literally lie on the fitting straight line, which confirms the validity of the assumption.

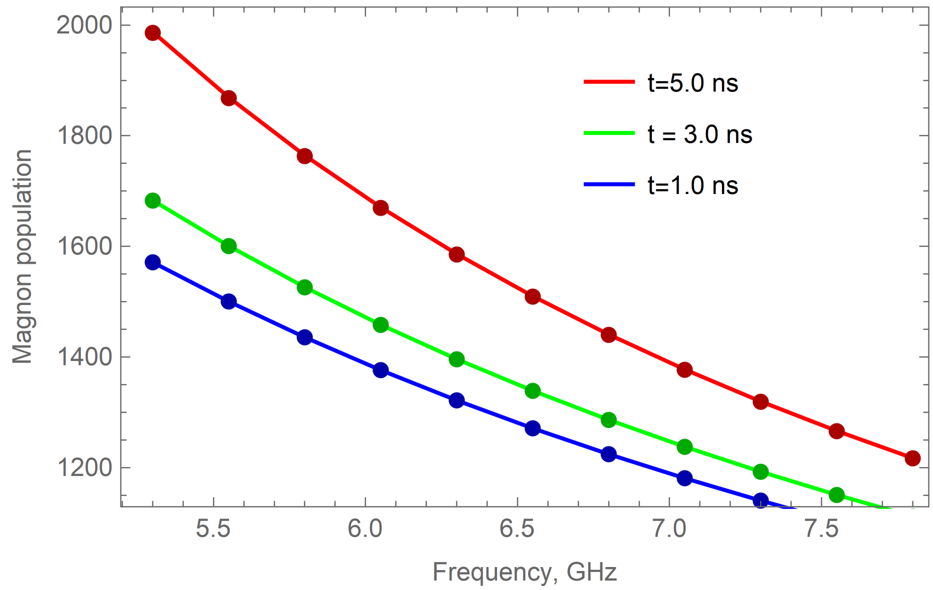


Figure 4.4: The distribution of the population number of magnons over frequencies at different times after the start of rapid cooling. Data points represent the simulated population distribution, and the solid lines represent the population numbers expected in the case of quasi-equilibrium magnon gas (Bose-Einstein distribution). The data points and the corresponding curves coincide, which confirms the validity of the assumption.

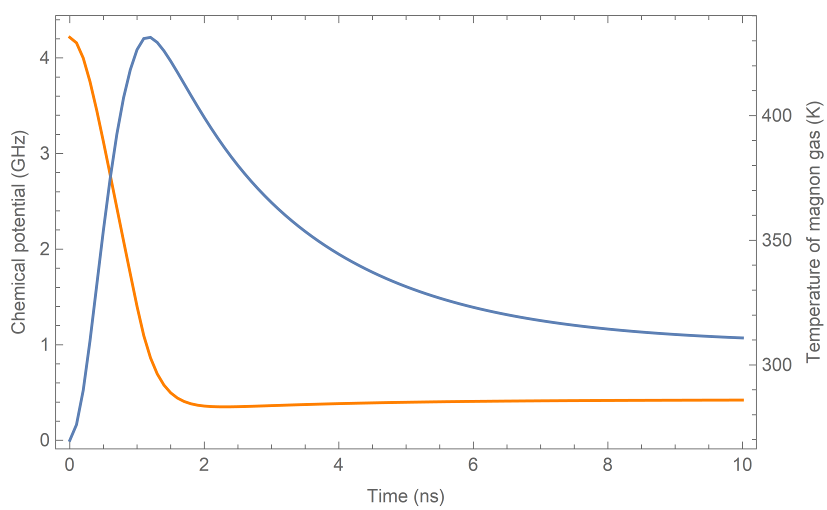


Figure 4.5: The time profiles of the effective parameters of the magnons gas, obtained from the simulated data using the linearization procedure described above.

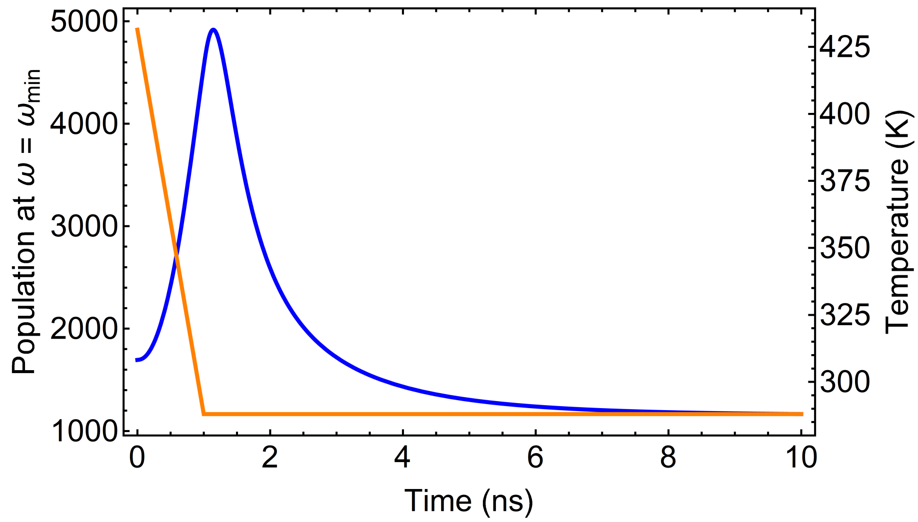


Figure 4.6: The population of magnons at the minimum energy $\hbar\omega_{\min}$ of propagating magnons (blue line) and the lattice temperature (orange line) as a function of time after the start of rapid cooling.

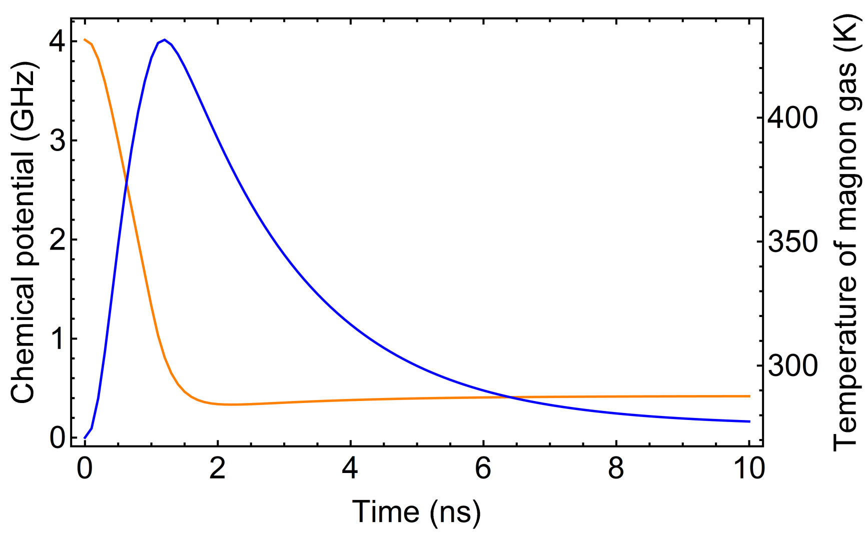


Figure 4.7: The change in time of effective chemical potential $\mu$ (blue line) and effective temperature $T$ (blue line) of rapidly cooling magnon gas. Horizontal axis shows the time passed since the start of rapid cooling.

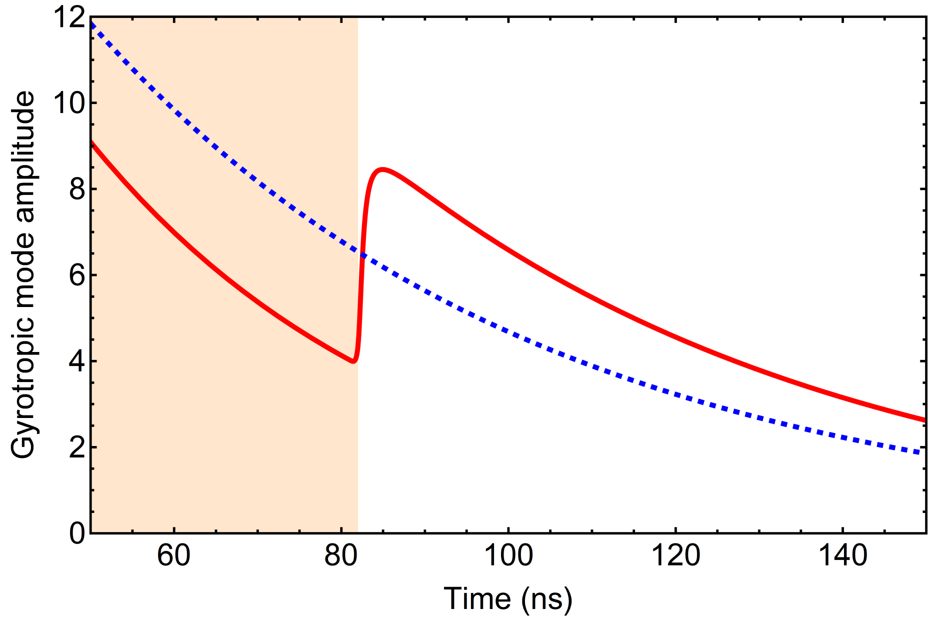


Figure 4.8: Change of the average amplitude of the gyrotropic mode in time with (red line) and without (blue line) rapid cooling. The time scale represents the time since the start of simulation, and the orange area represents the period when a heating pulse was applied.

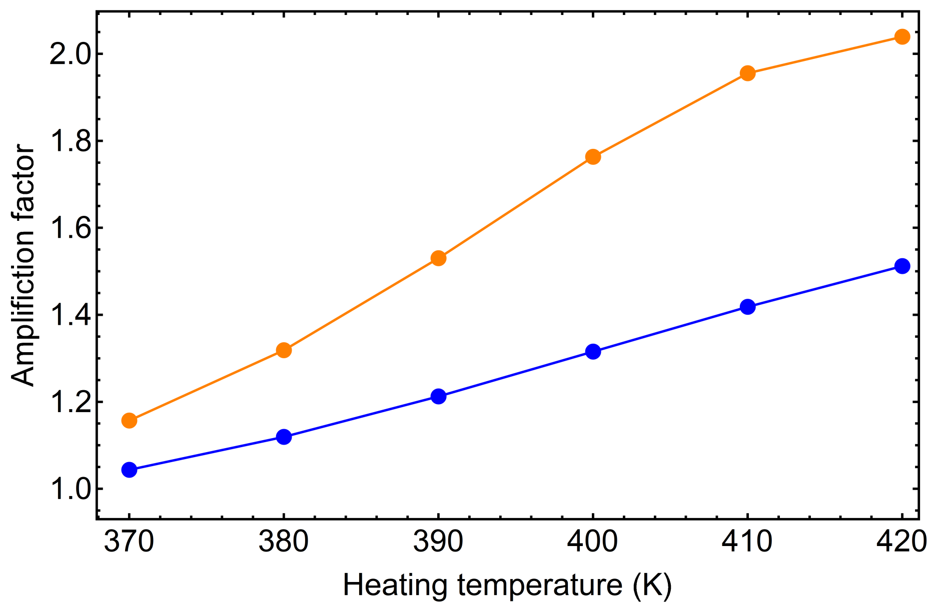


Figure 4.9: Dependence of amplification gain on the heating temperature calculated using amplitudes from the simulated data directly (blue dots) and using Eq. (4.89) (orange dots). The results obtained in two ways are qualitatively the same and show that the amplification factor increases with the increase of heating temperature.

# CHAPTER FIVE

# BOSE-EINSTEIN CONDENSATION OF RAPIDLY COOLING MAGNONS GAS IN ANTIFERROMAGNETS

This chapter discusses the possibility of creating Bose-Einstein Condensate (BEC) of magnons in Antiferromagnetic (AFM) materials using method of rapid cooling. Typically, this method is used for formation of a magnonic BEC only in Ferromagnetic (FM) crystals. Here application of the same method to an unbiased AFM film is analyzed in theory. Then, series of simulations is performed considering the sample made of NIO with Antiferromagnetic Resonance (AFMR) frequency of the lower branch of the magnon spectrum of around 0.2 THz [33], [34]. NiO is a room temperature antiferromagnetic insulator with biaxial, or easy-plane, anisotropy. It has two distinct AFMR frequencies and, therefore, two distinct branches of AFM magnons. Thus, the AFM magnonic branches are not equally populated, and cannot compensate each other. NiO has two magnonic eigenmodes, and both of them demonstrate elliptical precession which gives rise to an oscillating magnetization component [33]. This oscillating component ensures generation of oscillating dipolar field, and, therefore, results in the terahertz frequency radiation.

The results discussed in this chapter were previously presented in conference presentations [15], [16], [17] and invited talk [18].

## 5.1 Theoretical description of non-equilibrium magnon gas dynamics

The spectrum of magnons in AFM materials consists of two branches due to the fact that AFM has two magnetic sublattices. The dispersion relation for each branch can be written as:

$$\omega_{\mathbf{k}} = \sqrt{\omega_0^2 + c^2 k^2}, \tag{5.1}$$

where $\omega_0$ is the AFMR frequency (gap in the AFM magnon spectrum) and $c$ is the limiting (at $k \to \infty$) speed of the AFM magnons. For easy-plane antiferromagnets, like NiO, the magnon gaps $\omega_0$ in the two magnon branches significantly differ (several hundred GHz *vs* a few THz). For the processes considered in this work only the lower magnon branch, which has a higher thermal magnon population and may undergo Bose-Einstein condensation, is important.

A traditional way to describe interaction between magnons in a magnonic gas is by using kinetic equation for magnon population numbers $n_{\mathbf{k}} = n_{\mathbf{k}}(t)$ [35]:

$$\frac{dn_{\mathbf{k}}}{dt} = -2\Gamma_{\mathbf{k}}(n_{\mathbf{k}} - n_{\mathbf{k}}^{(0)}) + G_{\mathbf{k}}\,. \tag{5.2}$$

The first term in the right-hand side of this equation describes magnon-lattice interaction, while the second term – interactions within the magnonic subsystem. Here $\Gamma_{\mathbf{k}} = \alpha_{\mathrm{G}}\omega_{\mathbf{k}}$ is the magnon damping rate due to the magnon-lattice interaction, ($\alpha_{\mathrm{G}}$ is the dimensionless Gilbert damping parameter) and $n_{\mathbf{k}}^{(0)}$ is the Bose-Einstein thermal equilibrium distribution at the lattice temperature and zero chemical potential. $G_{\mathbf{k}}$ in Eq. (5.2) describes interaction between magnons via a 4-magnon scattering processes, and can be written as:

$$G_{\mathbf{k}} = \sum_{\mathbf{123}} \left|T_{\mathbf{k1},\mathbf{23}}\right|^2 f_{\mathbf{k1},\mathbf{23}}, \tag{5.3}$$

where sum is taken over all possible combinations of magnons satisfying energy ($\omega_{\mathbf{k}} + \omega_{\mathbf{1}} = \omega_{\mathbf{2}} + \omega_{\mathbf{3}}$, $\omega_{\mathbf{1}} \equiv \omega_{\mathbf{k}_1}$) and momentum ($\mathbf{k} + \mathbf{k}_1 = \mathbf{k}_2 + \mathbf{k}_3$) conservation laws. $T_{\mathbf{k1},\mathbf{23}}$ is the 4-magnon interaction coefficient independent of magnon population, and the term $f_{\mathbf{k1},\mathbf{23}}$ describes dependence of the 4-magnon scattering on the population of magnon states (see Eq. (2.1.29a) on p. 71 in [35]:

$$f_{\mathbf{k1},\mathbf{23}} = (n_{\mathbf{k}} + 1)(n_{\mathbf{1}} + 1)n_{\mathbf{2}}n_{\mathbf{3}} - n_{\mathbf{k}}n_{\mathbf{1}}(n_{\mathbf{2}} + 1)(n_{\mathbf{3}} + 1)\,. \tag{5.4}$$

The model Eq. (5.2) may be used to analyze non-equilibrium magnon dynamics during processes of heating and cooling. In this case, the equilibrium Bose-Einstein distribution $n_{\mathbf{k}}^{(0)}$ is determined by the instantaneous lattice temperature $T_l(t)$, thus leading to the explicit time dependence of the model Eq. (5.2) and development of non-equilibrium time-dependent magnon states $n_{\mathbf{k}}(t)$.

Direct analysis of Eqs. (5.2)-(5.4) is difficult because one needs to consider all the possible interactions contributing to the population of magnons $n_{\mathbf{k}}$ to find the interaction term $G_{\mathbf{k}}$, and, with account of momentum and energy conservation laws, the summation in Eq.(5.3) becomes a five-dimensional sum. Thus, direct numerical simulations of the model Eqs. (5.2)-(5.4) is unfeasible at the present time, and one has to employ certain approximate methods to analyze nonlinear magnon-magnon interactions involving the whole thermally excited spectrum of magnons.

The estimated magnon-magnon relaxation rate for NiO is $\Gamma_m = 6.9 \cdot 10^8$ 1/s at the bottom of the spectrum at room temperature and rapidly increases with the increase of magnon frequency ($\propto \omega^4$) and temperature ($\propto T^5$), see (4.11) in [36]. This value is close to the observed AFMR linewidth in high quality NiO samples with $\alpha_G \sim 10^{-4}$. Thus, we may assume that the magnon-magnon interaction is a dominant process in relaxation of room-temperature magnon gas containing magnons frequencies up to $f_T = k_B T/h \sim 6$ THz. Respectively, we shall assume that the magnon-magnon term $G_k$ in Eq. (5.2) is much stronger than the magnon-lattice interaction described by $\Gamma_k$ rate, and employ two-time model in which fast time scale is related to the intrinsic magnon dynamics ($G_k$), while the slow time scale describes magnon-lattice interaction ($\Gamma_k$).

One can assume that the magnon-magnon interaction is so fast compared to the magnon-lattice interaction, that the magnon distribution $n_{\mathbf{k}}$ is very close to internal equilibrium (quasi-equilibrium state). This quasi-equilibrium state can be approximately described by the standard Bose-Einstein distribution:

$$n_{\mathbf{k}} = n_0(\omega_{\mathbf{k}}, T, \mu) = \frac{1}{\exp\left(\dfrac{\hbar\omega_{\mathbf{k}} - \mu}{k_B T}\right) - 1}, \tag{5.5}$$

where $k_B$ is the Boltzmann constant and $\hbar$ is the reduced Planck constant ($\hbar = h/(2\pi)$). The quasi-equilibrium approximation also implies that the magnon temperature $T$ may differ from the lattice temperature $T_l$, and magnon chemical potential $\mu$ may be non-zero.

The magnon-magnon scattering processes Eq. (5.3) conserve the particle density

$$N(T,\mu) = \int_{\omega_0}^{\infty} n_0(\omega, T, \mu) D(\omega) d\omega \tag{5.6a}$$

and the energy density

$$E(T,\mu) = \int_{\omega_0}^{\infty} \hbar\omega n_0(\omega, T, \mu) D(\omega) d\omega \tag{5.6b}$$

of the magnon gas.

Here $D(\omega)$ is the density of magnonic states determined by the dispersion relation of the AFM magnons Eq. (5.1). The dependence of the density of states $D(\omega)$ on the magnon spectrum is implicit and has the form

$$D(E) = \frac{\partial}{\partial E}\left(\frac{k^3}{6\pi^2}\right), \tag{5.7}$$

where $E = \hbar\omega$ is the magnon energy. From Eq. (5.1) one can extract the dependence $k(E)$:

$$k(E) = \frac{1}{\hbar c}\sqrt{\left(\frac{E}{E_0}\right)^2 - 1}, \tag{5.8}$$

where $E_0 = \hbar\omega_0$ is the minimum energy of the AFM magnon spectrum.

By substituting Eq. (5.8) into Eq. (5.7) and simplifying the expression we get

$$D(\omega) = \frac{\omega}{2\pi^2 c^3}\sqrt{\omega^2 - \omega_0^2}, \tag{5.9}$$

It should be noted, that densities of states $D(\omega)$ and $D(E)$ are equivalent and the variable chosen (either angular frequency $\omega$ or magnon energy $E$) only affects the parameter over which integration in Eqs. (**??**) and (5.6b) is done. In numerical simulation, calculations was done using dimensionless parameters, which removes the need of choosing one variable over another one.

The particle $N$ and energy $E$ densities vary on the slow time scale due to the magnon-lattice interactions. Using the kinetic equations Eq. (5.2), the rate of change of these quantities can be found as:

$$\frac{dN}{dt} = -2\alpha_{\mathrm{G}} \int_{\omega_0}^{\infty} \omega u(\omega) D(\omega) d\omega \,, \tag{5.10a}$$

$$\frac{dE}{dt} = -2\alpha_{\mathrm{G}} \int_{\omega_0}^{\infty} \hbar\omega^2 u(\omega) D(\omega) d\omega, \tag{5.10b}$$

where $u(\omega)$ is the excess of the magnon population over the lattice equilibrium value:

$$u(\omega) = n_0(\omega, T, \mu) - n_0(\omega, T_{\mathrm{l}}, 0). \tag{5.11}$$

Equations (5.10) together with Eqs. (5.6) form a system of implicit differential equations for the magnon gas temperature $T$ and chemical potential $\mu$. It should be noted, that rate equations (5.10) do not contain the term describing magnon-magnon scattering, because four-wave magnon-magnon scattering processes conserve the particle density $N$ and the energy density $E$. Various magnon processes may be studied by using different time dependencies of the lattice temperature $T_l(t)$. This model can also be easily generalized to study interaction of a magnon gas with a thermal bath at a non-zero chemical potential (e.g., contact of a magnetic sample with a normal metal having a non-zero spin accumulation).

The above presented model is applicable only below the threshold of the Bose-Einstein condensation (BEC) ($\mu < \hbar\omega_0$). Above this threshold ($\mu = \hbar\omega_0$), Eqs. (5.6) should be replaced with:

$$N = \int_{\omega_0}^{\infty} n_0(T, \hbar\omega_0, \omega) D(\omega) d\omega + N_{\text{BEC}}\,, \tag{5.12a}$$

$$E = \int_{\omega_0}^{\infty} \hbar\omega n_0(T, \hbar\omega_0, \omega) D(\omega) d\omega + \hbar\omega_0 N_{\text{BEC}}\,, \tag{5.12b}$$

where $N_{\text{BEC}}$ is the BEC density. A similar modifications are also required for Eqs. (5.10):

$$\frac{dN}{dt} = -2\alpha_{\text{G}} \left[ \int_{\omega_0}^{\infty} \omega u(\omega) D(\omega) d\omega + \omega_0 N_{\text{BEC}} \right], \tag{5.13a}$$

$$\frac{dE}{dt} = -2\alpha_{\text{G}} \left[ \int_{\omega_0}^{\infty} \hbar\omega^2 u(\omega) D(\omega) d\omega + \hbar\omega_0^2 N_{\text{BEC}} \right], \tag{5.13b}$$

where $u(\omega)$ should be evaluated at $\mu = \hbar\omega_0$.

To describe both sub-critical ($\mu < \hbar\omega_0$, $N_{\text{BEC}} = 0$) and super-critical ($\mu = \hbar\omega_0$, $N_{\text{BEC}} > 0$) regimes in the same simulation, it is more convenient to use $N$ and $E$ as primary dynamical parameters of the magnon gas, and treat $T$, $\mu$, and $N_{\text{BEC}}$ as functions of $N$ and $E$ (implicitly defined by Eqs. (5.6) and (5.12)). This approach is used in the current work.

## 5.2 Results and discussion

Based on the presented above approach, a series of numerical simulations have been performed in Wolfram Mathemaica. In simulations, nickel oxide (NiO) was used as an AFM material. While the intrinsic Gilbert damping of NiO is around $6 \times 10^{-4}$ [34] and varies slightly depending on the sample being made of mono- or polycrystalline NiO [37], its extrinsic damping can be one order higher due to influence of the experimental environment [34]. The high quality of the used antiferromagnetic sample (caused by its monocrystalline structure) is an important pre-condition for the formation of the BEC of AFM magnons, because the presence of disorder in the atomic structure of the AFM sample will lead to the increase of damping, and will negatively impact the creation of the

Table 5.1: Material parameters of NiO used in simulations.

| **Parameter** | **Description** | **Simulation value** |
|---|---|---|
| $H_e$ | Exchange field | 968.4 T |
| $H_{ax}$ | in-plane anisotropy field | 635 mT |
| $H_{az}$ | out-of-plane anisotropy field | 11 mT |
| $a_l$ | lattice parameter | 4.177 Å |

AFM BEC. In the simulations, the value $\alpha_G = 1.5 \times 10^{-3}$ for the Gilbert damping of NiO has been used to account for possible increase of damping.

To evaluate AFM spectrum and density of states numerically, parameter $c$ in Eq. (5.1) has been calculated using material parameters of NiO. Considering the expression for lower branch of NiO spectrum in [33], the value of parameter $c$ can be calculated as

$$c = \left(\frac{a_l}{2}\gamma H_E,\right)^2 \tag{5.14}$$

where $a_l$ is the lattice parameter of NiO, $\gamma$ is the gyromagnetic ratio, and $H_E$ is the magnitude of the exchange field of NiO. The numerical values of material parameters used to calculate the minimum frequency of the AFM magnon spectrum and parameter $c$ are shown in the Table 5.1.

NiO has bi-axial anisotropy, which means that the two branches of AFM magnon spectrum have different minimum frequencies (0.21 THz and 1.1 THz). The density of states Eq. (5.1), which we used in our simulations, describes only one AFM magnon branch (branch with lower AFMR frequency $\omega_0/(2\pi) = 0.21$ THz). The higher magnon branch is not important for the process of rapid cooling of magnon gas and formation of magnon BEC since its gap frequency is several times higher, which justifies our simplifying approximation.

The process of rapid cooling of magnon gas is very sensitive to the rate of change of the lattice temperature $T_l(t)$. For slow, quasi-static changes of $T_l(t)$ the magnons thermodynamic parameters $T(t)$ and $\mu(t)$ will follow instantaneous values of the corresponding lattice parameters. In such a case, obviously, $\mu(t) = 0$, and no condensation of magnons is possible.

During the process of rapid cooling the way temperature decreases may be as important as the cooling time. In a simplest case one could utilize linear cooling when during the cooling time the lattice temperature drops from the heating temperature to the cooling temperature in a linear way. However, typically no transition process in nature happens in such a way. Considering that magnon related processes in AFM happen on much shorter timescale than in FM, the cooling should be implemented in a nonlinear way. In simulations presented here, a simple exponential formula has been used to describe the change of lattice temperature $T_l$:

$$T_l(t) = T_c + (T_h - T_c)\exp\left(-\frac{t}{\tau}\right). \tag{5.15}$$

Here $T_h$ is the initial temperature of the lattice before the cooling starts (heating temperature), $T_c$ is the equilibrium temperature after cooling at $t \to \infty$ (cooling temperature), and $\tau$ is the cooling time of the lattice. The visualization of the cooling process is depicted in Fig. 5.1.

The system of differential equations (5.6) is not easy to solve numerically because the right hand side does not depend on the total magnon density $N$ and total magnon energy density $E$ explicitly. Instead, the integral in the right hand side depends on effective temperature $T$ and chemical potential $\mu$ of the AFM magnon gas. The way to solve this problem is to pre-calculate the value of the integral for all possible values of

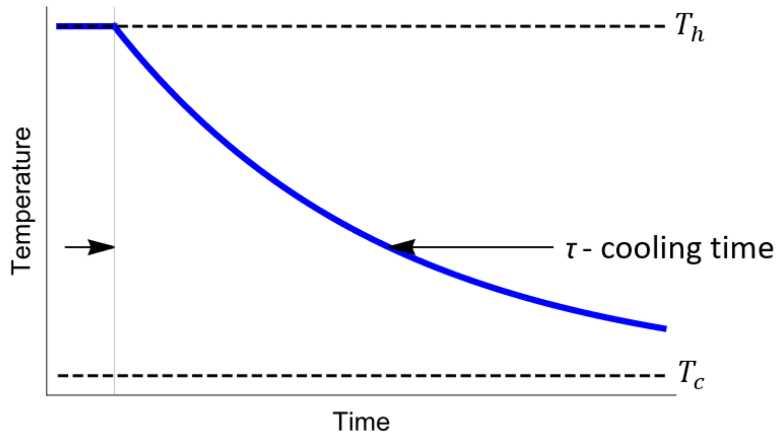


Figure 5.1: Visulization of exponential change of temperature during the rapid cooling of AFM. The solid blue line shows the temporal profile of the lattice temperature $T_\mathrm{l}$, while the horizontal dashed lines show the levels of heating temperature $T_\mathrm{h}$ and the cooling temperature $T_c$, and the arrows mark the cooling time $\tau$.

temperature $T$ and chemical potential $\mu$, which then allows one to make a connection between the integral and parameters $N$ and $E$ since they also depend on $T$ and $\mu$. This way, although the equations are written for the total magnon density $N$ and total magnon energy density $E$, temperature and chemical potential of the magnon gas act as intermediate variables in the solution process.

Fig. 5.2 shows examples of temporal profiles of magnon temperature $T(t)$ and chemical potential $\mu(t)$ during the rapid cooling process for different lattice cooling times $\tau$. As one can see, the magnon temperature $T(t)$ only slightly deviates from the instantaneous lattice temperature $T_\mathrm{l}(t)$, with maximum deviation being of the order of 1 K for the shortest cooling time $\tau = 0.12$ ns.

The magnon chemical potential, on the other hand, shows strong dependence on the cooling time $\tau$. It rapidly increases during the first $\sim 0.02$ ns of the rapid cooling, after which it relatively slowly decays to the thermodynamically equilibrium value $\mu = 0$. The

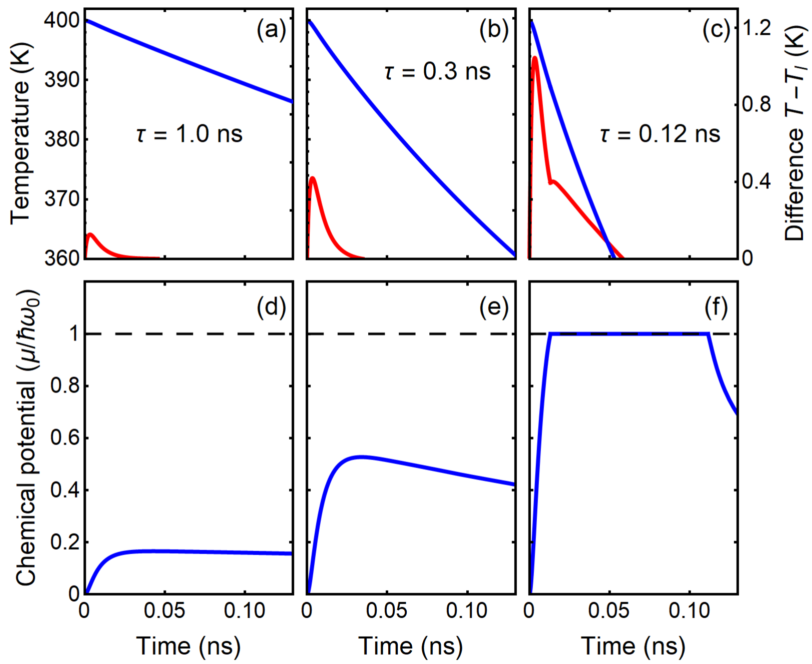


Figure 5.2: Temporal profiles of temperature (panels (a)-(c)) and chemical potential (panels (d)-(f)) of the magnon gas in the process of rapid cooling for different lattice cooling times $\tau$. The red solid lines in (a)-(c) show the difference between the magnon $T(t)$ and lattice $T_{\mathrm{l}}(t)$ temperatures (right scale). The horizontal dashed lines in (d)-(f) mark the maximum possible chemical potential of magnons $\mu = \hbar\omega_0$. Heating temperature $T_{\mathrm{h}} = 400$ K, cooling temperature $T_{\mathrm{c}} = 288$ K.

maximum value of the chemical potential strongly depends on the cooling time $\tau$, and it reaches magnon gap energy $\mu = \hbar\omega_0$ for the cooling time $\tau = 0.12$ ns. In this case, AFM magnon BEC at the frequency $\omega = \omega_0$ is formed. It is interesting to note, that the temperature difference $T(t) - T_{\mathrm{l}}(t)$ demonstrates a kink at the point of BEC formation (see panel (c) in Fig. 5.2), which is indicative of the second-order phase transition in the magnon gas, associated with the change of its heat capacity.

The process of BEC formation in rapid cooling is further illustrated by Fig. 5.3, where we show temporal dependencies of the magnon chemical potential $\mu$ and BEC density (as percentage of the total magnon density) for different cooling times. As one can see, by speeding up the cooling process one can increase both the duration of the BEC pulse and its peak magnitude. The maximum BEC fraction may reach significant values of several percents of total magnon population if a sufficiently fast cooling ($\tau \simeq 0.05$ ns) is provided.

The duration of the BEC pulse and its peak magnitude depend not only on the cooling time $\tau$, but also on the cooling $T_c$ and heating $T_h$ temperatures. These dependencies are illustrated by Fig. 5.4 and Fig. 5.5.

From Fig. 5.4 one can see that the increase of heating temperature $T_h$ leads to an increase of the BEC pulse duration. The duration of BEc pulse nonlinearly depends on the cooling time and has a certain critical cooling time $\tau_{cr}$ below which the duration is zero, meaning, the cooling of the sample is not rapid enough and BEC of magnons does not form. The vertical black dashed line on Fig. 5.4 marks the cooling time $\tau = 0.13$ ns. This example illustrates important connection between critical cooling time $\tau_{cr}$ and the heating temperature $T_h$: at the heating temperature $T_h = 400$ k the cooling time $\tau = 0.13$ ns is enough for AFM magnon BEC to form, while at heating temperature $T_h = 380$ K the cooling time $\tau = 0.13$ ns is not enough for AFM magnon BEC formation.

In Fig. 5.5 the BEC pulse magnitude is characterized by the peak energy density $E_{BEC} = \hbar\omega_0 N_{BEC}$ rather than BEC density fraction used in Fig. 5.3, because the peak energy density is a convenient parameter to use in practical applications of the AFM BEC as a source of the sub-THz-frequency radiation. For example, one can use the peak energy density $E_{BEC}$ to estimate the peak power of the sub-THz-frequency radiation extracted from the AFM magnon BEC.

As expected, the heating temperature $T_h$ has a positive correlation with both the peak energy and duration of the BEC pulse. As one can see from Fig. 5.4, it is possible to achieve BEC energy density of the order of $1\,\mathrm{kJ/m^3}$. This number allows one to estimate the maximum power $P_{BEC} = 2\Gamma_r E_{BEC} V_{AFM}$ of sub-THz radiation that can be extracted from the AFM BEC source. Here $\Gamma_r$ is the rate of radiative losses of the magnon BEC into external circuit or antenna, and $V_{AFM}$ is the volume of the AFM sample. Assuming that the AFM sample is a 5 nm thick NiO film with $100\,\mu\text{m} \times 100\,\mu\text{m}$ lateral sizes and BEC radiative losses are $\Gamma_r \sim \alpha_G \omega_0 \sim 1\,\text{ns}^{-1}$, the peak sub-THz power extracted from the BEC may reach 0.1 mW. This power can be increased by using, for example, the phenomenon of mutual synchronization in an array of AFM samples undergoing simultaneous rapid cooling. The typical duration of the sub-THz pulse for NiO is of the order of 0.1 ns, which should be sufficient for many practical applications.

Another important thing illustrated by the Fig. 5.4 and Fig. 5.5 is the threshold nature of the BEC formation, which is expected since the criterion of the chemical potential of the magnon gas reaching the spectral gap value is the threshold itself. It means that there is a certain critical cooling time $\tau_{cr}$ required to achieve BEC condensation of magnons during rapid cooling of an AFM sample.

The dependence of the critical cooling time $\tau_{cr}$ on the heating $T_h$ and cooling $T_c$ temperatures is illustrated by Fig. 5.6: each line in this figure has been calculated for constant temperature difference $T_h - T_c$. As one can see, the critical cooling time $\tau_{cr}$ rapidly increases with the decrease of the cooling temperature $T_c$, meaning that working at lower $T_c$ relaxes the conditions for magnon BEC formation. In particular, critical cooling time at liquid nitrogen temperature (77 K) is about three times longer than at the room temperature (288 K).

## 5.3 Conclusion

Thermal heating, and subsequent rapid cooling of an AFM sample can form a magnon BEC state and generate a short radio-pulse of a sub-THz carrier frequency with the duration of about 0.1 ns and peak power reaching 0.1 mW. The cooling times required for this process are rather short ($\tau_{cr} \sim 0.1$ ns for NiO at room temperature), but can be substantially increased by using cryogenic cooling temperatures. This effect may find practical applications in the development of compact sources of coherent sub-THz-frequency radiation.

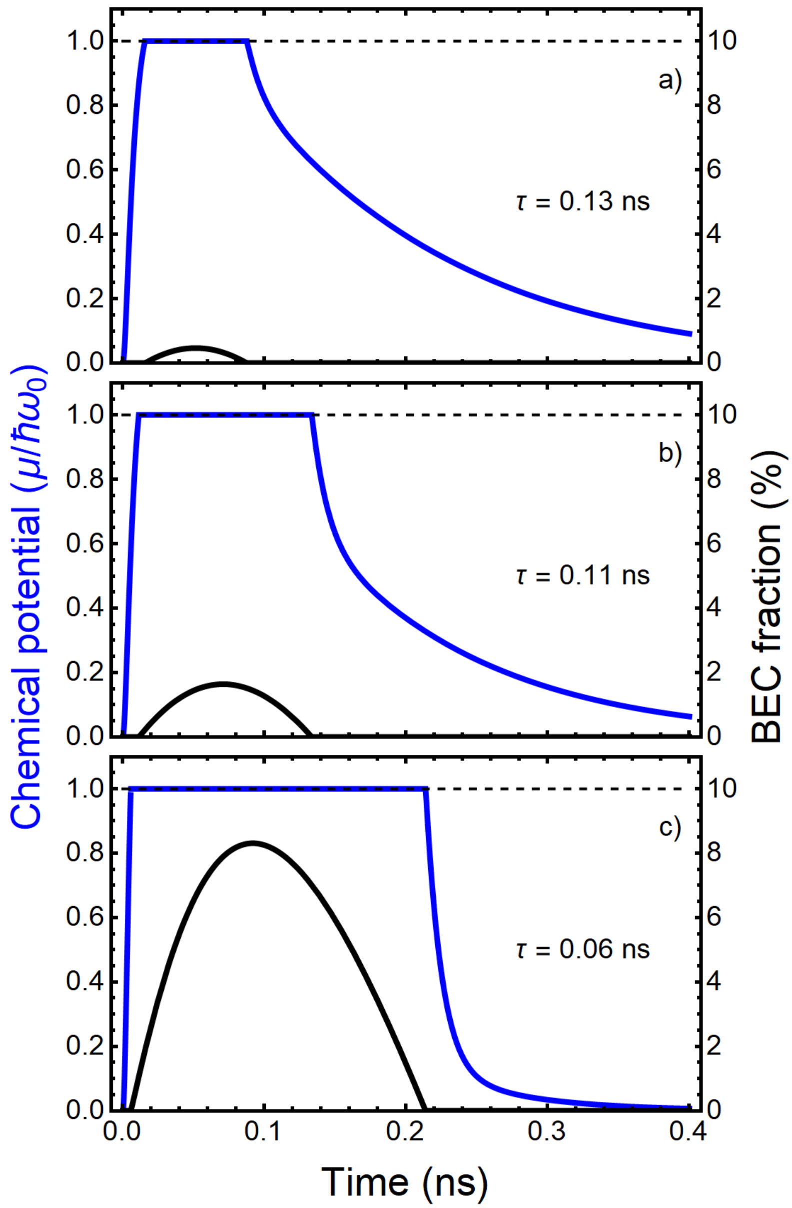


Figure 5.3: Temporal profiles of the chemical potential of the magnons gas (blue lines, left axis) and the BEC fraction relative to the total magnon density (black lines, right axis) for different cooling times $\tau$. The horizontal dashed line marks the level of the minimum energy of magnons.

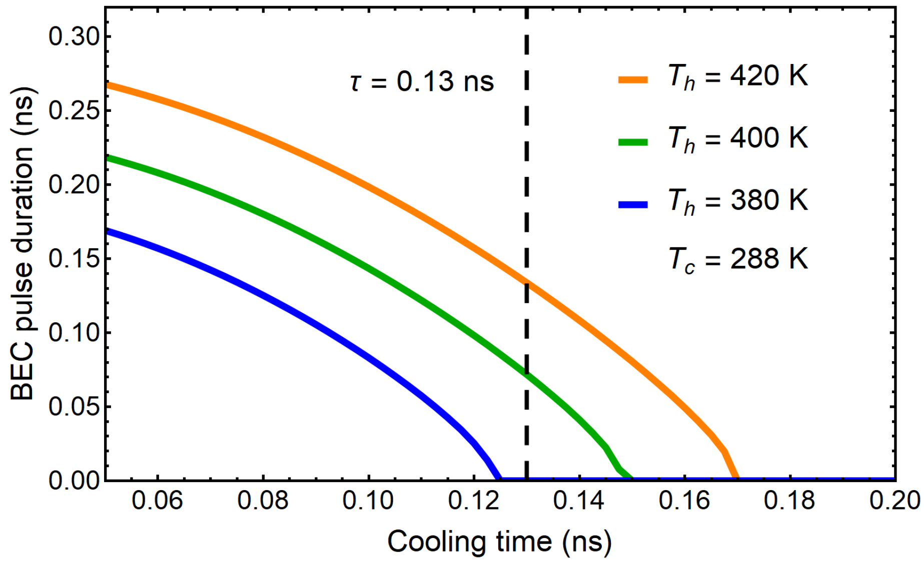


Figure 5.4: Dependence of the peak magnon BEC energy density on the cooling time for different heating temperatures $T_\mathrm{h}$ and the cooling temperature of $T_\mathrm{c} = 288$ K. The vertical black dashed line marks the cooling time of 0.13 ns.

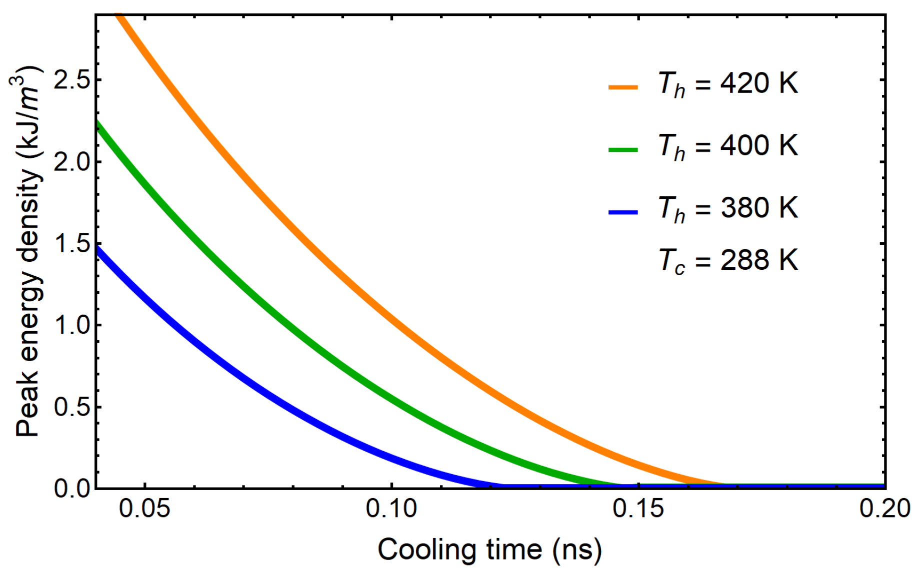


Figure 5.5: Dependence of the magnon BEC pulse duration on the cooling time for different heating temperatures $T_\mathrm{h}$ and the cooling temperature of $T_\mathrm{c} = 288$ K.

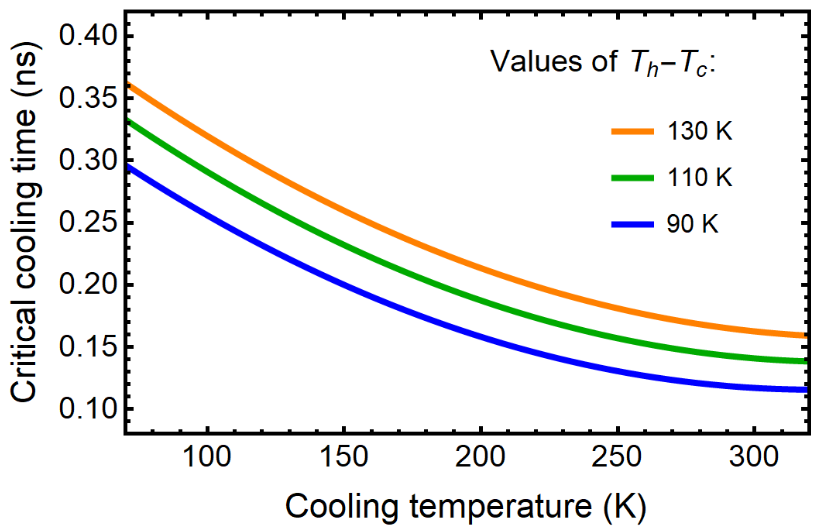


Figure 5.6: Dependence of the critical cooling time $\tau_{\rm cr}$ required to achieve BEC of AFM magnons on the cooling temperature $T_{\rm c}$ (different lines correspond to different temperature differences $T_{\rm h} - T_{\rm c}$).

# CHAPTER SIX

# CONCLUSIONS

Bose-Esintein condensation of magnons is a collective phenomenon which can be observed as spontaneous significant accumulation of magnons at the bottom of the spectrum due to transfer of magnons to the same quantum state. The BEC formed possesses dynamic properties, related to propagation of the BEC magnon density. It also exhibits nonlinear properties manifesting themselves through stability of BEC due to interaction between magnons in BEC, as well as interaction of BEC with other magnetic excitations present in the considered sample.

In the first study (Chapter 3), anisotropic nature of dynamic properties of BEC is analyzed and a simple way to describe them is proposed. The wave-particle duality of magnons is discussed through a similarity between a magnon in a film sample and a particle in an infinite potential well. For a complete picture, nonlinear properties of BEC are investigated with taking into account peculiarities of magnon modes at the bottom of the spectrum. The results obtained confirm the nature of BEC stability and suggest the the dependence on th geometric parameters of the sample. The final results are presented in an easy to analyze form and can be used for quick estimations.

The nonlinear properties of magnons are further discussed in more detail (Chapter 4) when an interaction between rapidly cooling magnons gas and an isolated low-frequency mode is investigated. The changes in the magnon gas in the process of BEC formation are illustrated and their possible influence on an isolated low-frequency mode is analyzed in theory and through numerical simulation of the interaction. Coherency of interacting mangons modes is discussed and it is shown that the low-frequency mode undergoes coherent amplification despite the interaction with thermal (incoherent magnons).

The third study (Chapter 5) is dedicated to generalization of the method of rapid cooling and analyzes its applicability in the case of a sample made of AFM material. A model for description of temporal evolution of the magnon gas is presented and is used to establish conditions required for BEC formation. The influence of parameters of the rapid cooling procedure on the BEC formation is analyzed. According to the findings, the BEC created this way may be suitable for practical applications in the area of sub-THz devices, specifically, for generation of ultra-short sub-THz frequency pulses.

The results obtained show a different point of view on some of the known properties of magnon BEC and create a path to new areas of research. The theoretical work presented in the dissertation provides tools for description and analysis of new phenomena related to BEC formation in the magnon gas, in both FM and AFM materials. The numerical simulation provided data helps to understand known BEC-related phenomena and suggests new practical applications for magnon BEC and their practical realization.

APPENDIX A

RADIATION SAFETY EXEMPTION LETTER

OAKLAND UNIVERSITY

Petro Artemchuk
Graduate Student, Applied and Computational Physics
Department of Physics, Oakland University

July 21, 2025

Re: Radiation Safety Approval for Dissertation

Dear Mr. Artemchuk:

I received your email request dated July 13, 2025, indicating that you require a Radiation Safety letter of exemption or approval for your dissertation project titled: **Bose-Einstein condensation of magnons in ferromagnets and antiferromagnets**.

You have explained to me that the data generated for your dissertation is aquired through mathematical derivations or numerical simulations. You are not conducting any experiments for your dissertation. No radioactive materials will be used and no radiation generating procedures will be conducted. Based on your description of work for your dissertation, Radiation Safety Approval is not required. If for any reason you decide that experiments with radioactive materials or radiation generating procedures are necessary, please contact me so I can guide you through the Radiation Safety Approval process.

Sincerely,

Domenico Luongo
Director- Research Compliance & Integrity, Radiation Safety Officer.

THE RESEARCH OFFICE
Wilson Hall, Room 530
371 Wilson Boulevard
Rochester, MI 48309-4486
(248) 370-4314
Fax: (248) 370-2973
oakland.edu/research

Figure A.1: Copy of the Radiation Safety exemption letter.

REFERENCES


[1] P. Artemchuk, V. Tyberkevych, and A. Slavin, “A simple model for the description of bose-einstein condensation of magnons at room temperature,” in *APS March Meeting 2021*, ser. Bulletin of the American Physical Society, vol. 66, American Physical Society, Mar. 2021, R38.00004.

[2] P. Artemchuk, V. Tyberkevych, and A. Slavin, “A model for description of linear properties and stability of bose-einstein condensate of magnons at room temperature,” in *2021 IEEE International Magnetic Conference (INTERMAG 2021)*, Apr. 2021.

[3] P. Artemchuk and V. Tyberkevych, “A simple model describing linear properties of bose-einstein conden-sate of magnons in thick magnetic films,” in *Sixth Annual Oakland University Graduate Student Research Conference*, May 2021.

[4] P. Artemchuk, V. Tyberkevych, and A. Slavin, “Approximate model describing stability and dynamic properties of room-temperature bose-einstein condensate of magnons,” in *The 2021 Around-the-Clock Around-the-Globe Magnetics Conference, Program Booklet*, Aug. 2021, p. 227.

[5] P. Artemchuk, V. Tyberkevych, and A. Slavin, “A model for description of linear properties and stability of bose-einstein condensate of magnons at room temperature,” Sep. 2021.

[6] P. Artemchuk, V. Tyberkevych, and A. Slavin, “Increase of a bullet mode lifetime due to interaction with a hot mag-non gas,” in *15th Joint MMM-Intermag Conference, Abstract Book*, Jan. 2022, p. 459.

[7] P. Artemchuk, V. Tyberkevych, and A. Slavin, “Influence of a hot magnon gas on a bullet mode lifetime via incoherent interaction,” in *APS March Meeting 2022*, ser. Bulletin of the American Physical Society, vol. 67, American Physical Society, Mar. 2022, B52.00005.

[8] P. Artemchuk, V. Tyberkevych, and A. Slavin, “Bullet mode stabilization in the presence of a hot magnon gas,” in *7th Conference on Magnonics*, Aug. 2022.

[9] P. Artemchuk, V. Tyberkevych, and A. Slavin, “Stabilization of a nonlinear spin wave bullet mode in the presence of a hot magnon gas,” in *The 2021 Around-the-Clock Around-the-Globe Magnetics Conference, Program Booklet*, Aug. 2022, p. 72.

[10] P. Artemchuk, V. Tyberkevych, and A. Slavin, “Amplification of the gyrotropic mode power via interaction with a hot magnon gas,” in *67th Annual Conference on Magnetism and Magnetic Materials, Abstract Book*, Nov. 2022, p. 223.

[11] P. Artemchuk, V. Tyberkevych, and A. Slavin, "Hot magnon gas as an amplifier of a localized low-frequency mode," in *APS March Meeting 2023*, ser. Bulletin of the American Physical Society, vol. 68, American Physical Society, Mar. 2023, Q57.00002.

[12] P. Artemchuk, V. Tyberkevych, and A. Slavin, "Magnon amplification of a localized low-frequency mode," in *APS Eastern Great Lakes Section (EGLS) Spring 2023 Meeting*, Apr. 2023.

[13] P. Artemchuk, V. Tyberkevych, and A. Slavin, "Thermodynamic magnonic maser," in *Magnetic Frontiers: Quantum Technologies, Abstract Book*, Apr. 2023, p. 43.

[14] P. Artemchuk, V. Tyberkevych, and A. Slavin, "Amplification of an isolated magnon mode in a rapidly cooling gas of magnons," in *13th International Symposium on Hysteresis Modeling and Micromagnetics (HMM 2023)*, Jun. 2023.

[15] P. Artemchuk, V. Tyberkevych, and A. Slavin, "Bose-einstein condensation of rapidly cooling magnon gas in antiferromagnets," in *2024 International Conference on Microwave Magnetics*, Jun. 2024.

[16] P. Artemchuk, V. Tyberkevych, and A. Slavin, "Bose-einstein condensation of magnons in antiferromagnets due to rapid cooling," in *The 2024 Around-the-Clock Around-the-Globe Magnetics Conference, Program Booklet*, Oct. 2024, p. 80.

[17] P. Artemchuk, V. Tyberkevych, and A. Slavin, "Bose-einstein condensation of magnons in antiferromagnets using method of rapid cooling," in *2025 Oakland University Graduate Student Research Conference*, Apr. 2025.

[18] P. Artemchuk, V. Tyberkevych, and A. Slavin, "Generation of subterahertz frequency pulses in an antiferromagnet using thermal pumping," Mar. 2025.

[19] O. Dzyapko, V. E. Demidov, S. O. Demokritov, G. A. Melkov, and A. N. Slavin, "Direct observation of bose–einstein condensation in a parametrically driven gas of magnons," *New Journal of Physics*, vol. 9, no. 3, pp. 64–64, Mar. 21, 2007, ISSN: 1367-2630. DOI: `10.1088/1367-2630/9/3/064`.

[20] M. Schneider et al., "Bose–einstein condensation of quasiparticles by rapid cooling," *Nature Nanotechnology*, vol. 15, no. 6, pp. 457–461, Jun. 2020, ISSN: 1748-3387, 1748-3395. DOI: `10.1038/s41565-020-0671-z`.

[21] M. Schneider et al., "Control of the bose-einstein condensation of magnons by the spin hall effect," *Physical Review Letters*, vol. 127, no. 23, Dec. 2021, ISSN: 1079-7114. DOI: `10.1103/physrevlett.127.237203`.

[22] B. Divinskiy et al., "Evidence for spin current driven bose-einstein condensation of magnons," *Nature Communications*, vol. 12, no. 1, Nov. 2021, ISSN: 2041-1723. DOI: `10.1038/s41467-021-26790-y`.

[23] I. V. Borisenko, V. E. Demidov, V. L. Pokrovsky, and S. O. Demokritov, “Spatial separation of degenerate components of magnon bose–einstein condensate by using a local acceleration potential,” *Scientific Reports*, vol. 10, no. 1, Sep. 2020, ISSN: 2045-2322. DOI: 10.1038/s41598-020-71525-6.

[24] S. O. Demokritov et al., “Bose–einstein condensation of quasi-equilibrium magnons at room temperature under pumping,” *Nature*, vol. 443, no. 7110, pp. 430–433, Sep. 2006, ISSN: 1476-4687. DOI: 10.1038/nature05117.

[25] V. Tyberkevych, A. Slavin, P. Artemchuk, and G. Rowlands, *Vector hamiltonian formalism for nonlinear magnetization dynamics*, 2020. DOI: 10.48550/ARXIV.2011.13562.

[26] E. B. Sonin, “Spin superfluidity and spin waves in YIG films,” *Phys. Rev. B*, vol. 95, 144432 2017.

[27] M. Schneider et al., “Bose–einstein condensation of quasiparticles by rapid cooling,” *Nature Nanotechnology*, vol. 15, no. 6, pp. 457–461, Apr. 2020, ISSN: 1748-3395. DOI: 10.1038/s41565-020-0671-z.

[28] K. Y. Guslienko, G. R. Aranda, and J. Gonzalez, “Spin torque and critical currents for magnetic vortex nano-oscillator in nanopillars,” *Journal of Physics: Conference Series*, vol. 292, p. 012 006, Apr. 2011, ISSN: 1742-6596. DOI: 10.1088/1742-6596/292/1/012006.

[29] R. V. Verba et al., “Spin-wave excitation modes in thick vortex-state circular ferromagnetic nanodots,” *Physical Review B*, vol. 93, no. 21, Jun. 2016, ISSN: 2469-9969. DOI: 10.1103/physrevb.93.214437.

[30] J. Jorzick et al., “Spin wave wells in nonellipsoidal micrometer size magnetic elements,” *Physical Review Letters*, vol. 88, no. 4, Jan. 2002, ISSN: 1079-7114. DOI: 10.1103/physrevlett.88.047204.

[31] A. A. Serga et al., “Stabilization of a nonlinear magnonic bullet coexisting with a bose-einstein condensate in a rapidly cooled magnonic system driven by spin-orbit torque,” *Physical Review B*, vol. 104, p. L140405, 2021.

[32] D. Breitbach et al., “Stimulated amplification of propagating spin waves,” *Physical Review Letters*, vol. 131, p. 156 701, 2023.

[33] S. M. Rezende, A. Azevedo, and R. L. Rodríguez-Suárez, “Introduction to antiferromagnetic magnons,” *Journal of Applied Physics*, vol. 126, no. 15, Oct. 2019, ISSN: 1089-7550. DOI: 10.1063/1.5109132.

[34] R. Khymyn, I. Lisenkov, V. Tiberkevich, B. A. Ivanov, and A. Slavin, “Antiferromagnetic thz-frequency josephson-like oscillator driven by spin current,” *Scientific Reports*, vol. 7, no. 1, Mar. 2017, ISSN: 2045-2322. DOI: 10.1038/srep43705.

[35] V. E. Zakharov, V. S. L'vov, and G. Falkovich, *Kolmogorov Spectra of Turbulence I*. Springer Berlin Heidelberg, 1992, ISBN: 9783642500527. DOI: 10.1007/978-3-642-50052-7.

[36] D. Garanin, V. Lutovinov, and L. Panina, "The magnon-magnon interactions in easy-plane antiferromagnets," *Physica A: Statistical Mechanics and its Applications*, vol. 184, no. 3–4, pp. 523–557, Jul. 1992, ISSN: 0378-4371. DOI: 10.1016/0378-4371(92)90321-g.

[37] T. Moriyama, K. Hayashi, K. Yamada, M. Shima, Y. Ohya, and T. Ono, "Intrinsic and extrinsic antiferromagnetic damping in NiO," *Physical Review Materials*, vol. 3, no. 5, May 2019, ISSN: 2475-9953. DOI: 10.1103/physrevmaterials.3.051402.